# The Development of the Piedmont Front and Associated Outbreak of Severe Weather on 13 March 1986

STEVEN BUSINGER, WILLIAM H. BAUMAN III AND GERALD F. WATSON

*Department of Marine, Earth, and Atmospheric Sciences, North Carolina State University, Raleigh, North Carolina*

(Manuscript received 2 November 1990, in final form 18 March 1991)

ABSTRACT

An investigation was conducted of the mesoscale evolution of a quasi-stationary front, termed the *Piedmont front* owing to its location through the central Carolinas, and an associated outbreak of severe weather on 13 March 1986. Space–time relationships between mesoscale processes associated with the evolution of the surface front and the initiation of severe thunderstorms were studied utilizing the enhanced surface and upper-air observation networks deployed during the field phase of GALE. Surface streamline patterns, frontogenesis, and moisture-flux divergence were computed employing an objective analysis scheme.

Following the arrival at the Carolina coast of a coastal front, the Piedmont front rapidly developed along an axis of dilatation over the eastern margin of the Piedmont, while the coastal front gradually dissipated over the nearshore waters. A differential cloud cover across the Piedmont front resulted in enhanced solar insolation on the warm side of the front that strengthened frontogenesis and acted to further destabilize the atmosphere. On the afternoon of 13 March four severe thunderstorms formed in the vicinity of the Piedmont front. Three of the storms were located in the vicinity of mesolows that formed on the front. Subsequently, convection organized into a squall line along the front, as synoptic-scale forcing associated with a short-wave trough and cold front aloft (CFA) overtook the Piedmont front from the west.

Stability analyses indicate that on the synoptic scale only a weak to moderate potential for severe weather existed over portions of eastern North and South Carolina. However, fields of moisture-flux divergence show a mesoscale pattern of enhanced convergence well correlated with the locations of the severe thunderstorm cells. A schematic is presented that summarizes the principal factors involved in the development of the severe weather in this complex case.

## 1. Introduction

On 13 March 1986 strong frontogenesis occurred over the Carolinas and an associated outbreak of severe thunderstorms produced damaging winds and large hail. The severe weather occurred during the field phase of the Genesis of Atlantic Lows Experiment (GALE), providing an excellent opportunity to investigate the mesoscale interaction between observed frontogenesis, cyclogenesis, and squall-line initiation.

The synoptic conditions on 12 and 13 March 1986, as will be discussed in section 3 of this paper, were conducive both to cold-air damming and coastal frontogenesis. Mesoscale analyses (presented in section 4) show that a coastal front moved northwestward to the North Carolina coast early on 13 March and subsequently reformed inland over the Carolinas in a discontinuous shift. We refer to this new front as the *Piedmont front* owing to its location along the eastern margin of the Piedmont (see Fig. 1). It will be shown that in this case the development of the Piedmont front is closely tied to cold-air damming and differential solar heating across the front. Subsequently, a complex pattern of severe thunderstorms and a squall line developed along the front during the afternoon of 13 March.

The objectives of the research presented in this paper are to use the enhanced temporal and spatial resolution of the GALE observation network to:

(i) document the interaction of large-scale and mesoscale processes that lead to severe weather and squall-line development.

(ii) Investigate the mesoscale interactions between surface convergence, frontogenesis, cyclogenesis, and the location of severe weather development.

(iii) Identify signatures in the GALE mesoscale datasets that could be used in a prognostic sense for short-range forecasting of severe weather in similar cases.

(iv) Develop a conceptual schematic to portray key physical elements in the state of the atmosphere at the onset of severe weather.

When high-static-stability air emanates from a high pressure center over New England and encounters the east slopes of the Appalachians it is deflected southward, resulting in a dome of cold air along the eastern

*Corresponding author address:* Professor Steven Businger, Department of Marine, Earth, and Atmospheric Sciences, North Carolina State University, Raleigh, NC 27695-8208.


FIG. 1. Topography of the southeastern United States (Dirks et al. 1988).

slope of the mountains. Richwein (1980) referred to this phenomenon as "cold-air damming." Evaporation of precipitation as it falls through the cold air increases the baroclinicity across the leading edge of the cold dome, which often results in a boundary that distinguishes rain from snow or sleet (e.g., Forbes et al. 1987). A climatology of cold-air damming along the Appalachians shows that the Carolinas are a favored location for damming (Bell and Bosart 1988), especially in winter when up to five such events per month can be expected. Numerical weather prediction models have shown difficulty in forecasting the depth and duration of the dome of cold air associated with cold-air damming over the Carolinas (Forbes et al. 1987; Bell and Bosart 1988; Joseph Pelissier, personal communication). This deficiency may be the result of poor representations of the topography and/or insufficient resolution in the boundary layer of the models.

Coastal fronts are so named because coastal configuration, land–sea temperature contrast, and differential surface friction over water versus land play major roles in their formation, intensification, and dissipation (Bosart et al. 1972). The general features of coastal fronts have been documented in a number of important studies (Bosart 1975; Marks and Austin 1979; Ballentine 1980; Nielsen 1989; Nielsen and Nielley 1990). Low-level characteristics in the evolution of a coastal front along the North Carolina coast are the subject of a mesoscale study by Riordan (1990), who found a link between the location of the coastal front and the western edge Gulf Stream front, presumably driven by differential diabatic heating. Richwein (1980) observed that coastal fronts are generally oriented more closely parallel to terrain contours than to the coastline, evidence of a link between coastal-front formation and cold-air damming.

In the GALE case study presented in this paper, formation of a Piedmont front was associated with an outbreak of severe weather. Much research has been conducted on methods to predict severe weather events using synoptic-scale data (Fujita 1955; Galway 1956; George 1960; Miller 1967, 1972; David and Smith 1971). There has also been a great deal of success in recognizing relationships between synoptic-scale patterns and severe-weather outbreaks (e.g., Uccellini and Johnson 1979; Doswell 1980; Maddox and Doswell 1982; Johns 1984). A lack of meteorological data with mesoscale resolution, however, has limited efforts to investigate severe weather events triggered by mesoscale forcing. In the case presented in this paper it will be shown that the synoptic-scale pattern was not conducive to the development of severe weather. Therefore, forecasters did not anticipate severe thunderstorms until radar reflectivity data indicated heavy precipitation signatures <30 min prior to the outbreak of damaging thunderstorm winds and hail. The study presented in this paper, in the spirit of Doswell (1987), seeks to document the complex ways in which large-scale and mesoscale processes can interact, with a goal of improving our ability to recognize the potential for severe thunderstorm development locally in marginally unstable synoptic conditions.

## 2. The GALE observation network

Data available for this research includes a combination of standard and special observations at National Weather Service (NWS) and military stations plus observations from sites operated specifically for the GALE field program (Dirks et al. 1988). In addition, data and imagery were available from meteorological satellites in operation during GALE, including: *GOES-6*, *NOAA-9*, *NOAA-6*, *DMSP F-6*, and *Nimbus-7*.

Two data-gathering areas were of particular significance during GALE. The inner GALE area (Fig. 2) is approximately 500 km wide, centered on the Carolina coast, and extends 1000 km from Georgia to Virginia. Special observation systems deployed within this area include Portable Automated Mesonet (PAM) II, Doppler radars, ships, buoys, and Cross-chain Loran Atmospheric Sounding System (CLASS) sites (see Fig. 3a). The PAM-II network (Fig. 3b) consisted of 50 stations that provided 5-min-averaged meteorological surface observations (pressure, temperature, dewpoint temperature, precipitation amount and winds) over the

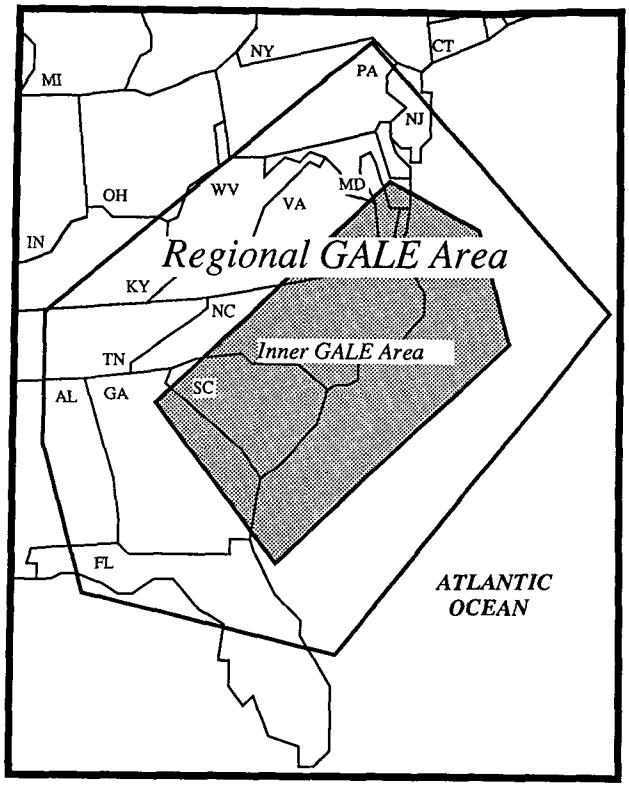


FIG. 2. Inner GALE area (shaded) and regional GALE area (outline) (Dirks et al. 1988).

coastal regions of the Carolinas and southern Virginia. Within this area, the larger end of the spectrum of the meso-$\beta$-scale (20–200 km) processes can be resolved, and smaller-scale processes can be examined.

The regional GALE area (Fig. 2) includes the southern Appalachians and extends from central Tennessee to 500 km offshore ($\sim$1000 km wide), and from Florida to New Jersey ($\sim$1500 km long). The regional GALE area data network allows examination of the meso-$\alpha$-scale processes of frontogenesis and cyclogenesis. Special measuring systems deployed within this area include: research aircraft, offshore Omega dropsondes, digitized NWS radar, and increased observations from standard upper-air stations. This area provides a geographical framework within which processes in the inner GALE area can be investigated in more detail.

## 3. Synoptic overview

On 12 March 1986 a backdoor cold front (Carr 1951; Bosart et al. 1973) moved southward along the east coast of the United States, across the GALE network in Virginia, and the Carolinas (not shown). This front propagated south along the east slopes of the Appalachians as the leading edge of high-static-stability air that emanated from a high pressure center over New England. The cold front stalled along the Georgia–South Carolina border and eastward over the Atlantic Ocean during the morning of 12 March. Analysis of buoy data over the Atlantic Ocean indicates that this front dissipated over the sea, while a separate coastal front formed in the vicinity of the Gulf Stream front through processes of differential surface fluxes over the warm Gulf Stream and the relatively cold nearshore waters along the Carolina coast (e.g., Riordan 1990). The evolution of this coastal front is the subject of a forthcoming paper (Allen Riordan, personal communication) and will not be treated in detail here.

The surface map for 0000 UTC 13 March (Fig. 4a) shows high pressure located over eastern Canada and a wedge of cold air to the east of the Appalachians that results hydrostatically in a surface-pressure ridge, conditions typical of cold-air damming and coastal frontogenesis. A warm front extends from a surface-low center over northwestern Missouri eastward into the Ohio Valley. This front wraps around the southern Appalachians and into Georgia as a cold front in response to the cold-air damming, where it connects with a region of frontogenesis over South Carolina. The original backdoor cold front has dissipated at this time, and a coastal front is analyzed along the Carolina coast.

Farther west, the surface analysis (Fig. 4a) shows a trough extending south from the Missouri low pressure center, through Arkansas and eastern Texas. As discussed in more detail in Hobbs et al. (1990), this feature has a history of being analyzed as a cold front by the National Meteorological Center (NMC), though its characteristics are those of a dry line at this time. Farther to the west a shallow arctic front separates downslope warmed air over Texas from colder air to the north. A squall line with associated extensive cloud shield is located well to the east of the surface trough (Figs. 4a and 5). Although frontogenesis can be inferred in the vicinity of the squall line, there is no history of a cold front at the surface in this location. Between 1800 UTC 12 March and 0000 UTC 13 March, 11 tornadoes were spawned along the Mississippi–Alabama border, including the first F4 storm of the year, in association with this squall line.

The 500-mb height and vorticity analysis for 0000 UTC 13 March (Fig. 4b) shows a closed low over Nebraska with maximum winds ($\sim$45 m s$^{-1}$) centered over the Mississippi–Alabama border. Weak negative vorticity advection (NVA) is occurring over the Carolinas at this time. Analysis at 700 mb (Fig. 6a) shows that the leading edge of the cold-air advection is located over Mississippi, well to the east of the wind shift at the surface, while the 12-h forecast of vertical velocity provided by the NMC nested grid model shows lifting in the region of the squall line (Fig. 6b).

A vertical cross section was constructed for 0000 UTC (Fig. 7) from Amarillo, Texas (AMA), to Waycross, Georgia (AYS), oriented roughly perpendicular to the axis of the squall line (refer to Fig. 8b). Cross-

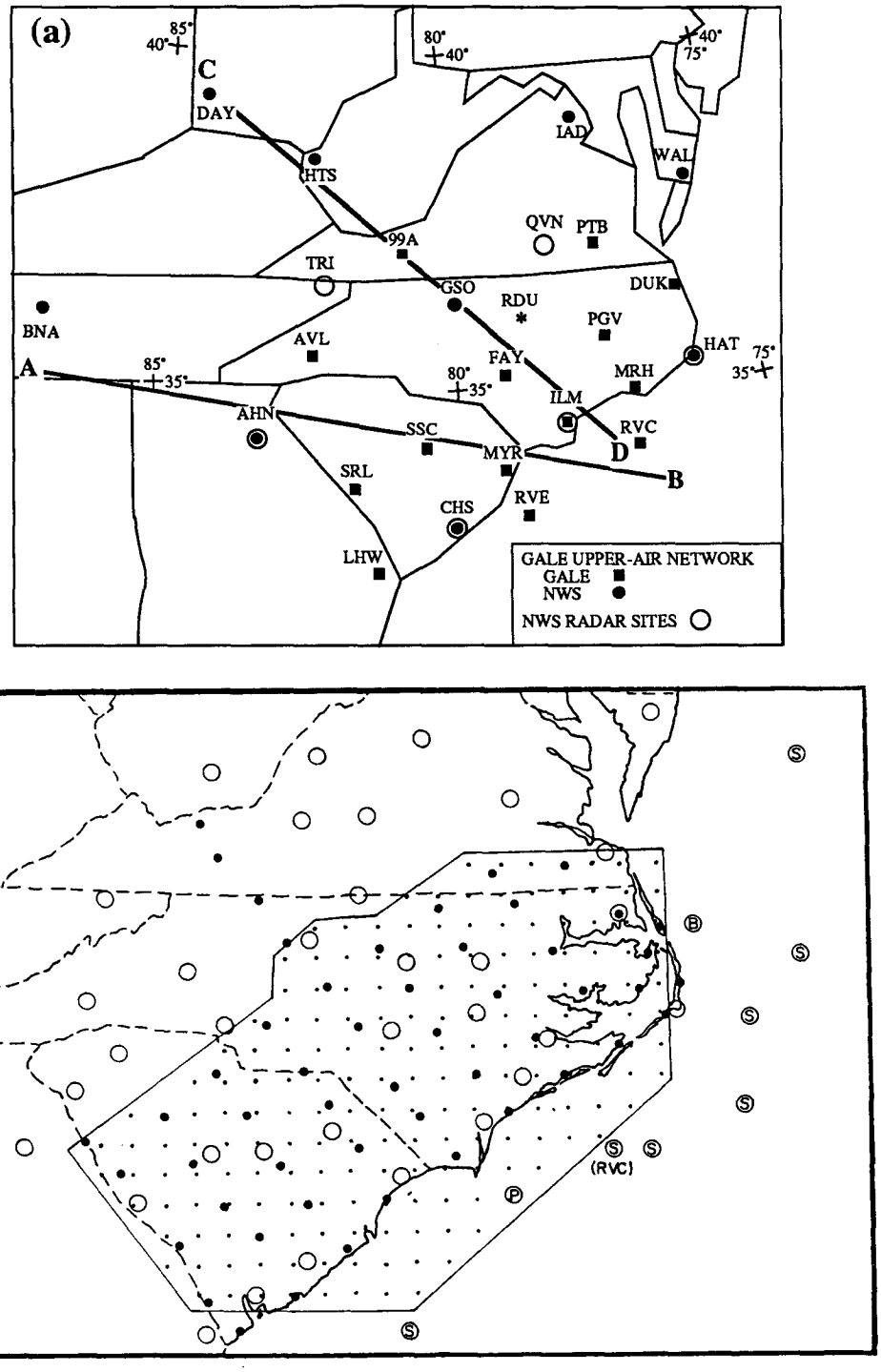


FIG. 3. (a) Regional GALE area showing locations of NWS and CLASS sounding sites, and the NWS forecast office at the Raleigh–Durham International Airport, North Carolina (RDU). RVC and RVE are the locations on 13 March 1986 of the NOAA research vessels *Cape Hatteras* and *Endeavor*, respectively. Heavy solid line AB indicates the location of the vertical cross section shown in Fig. 17. Heavy solid line CD indicates the location of the vertical cross section shown in Fig. 26. (b) Inner GALE area showing locations of PAM-II sites (large dots), NWS and FAA stations (open circles), ships of opportunity (circle S), buoys (circle B), and platforms (circle P). The outlined area shows the extent of the Barnes analysis grid, and small dots indicate grid points.

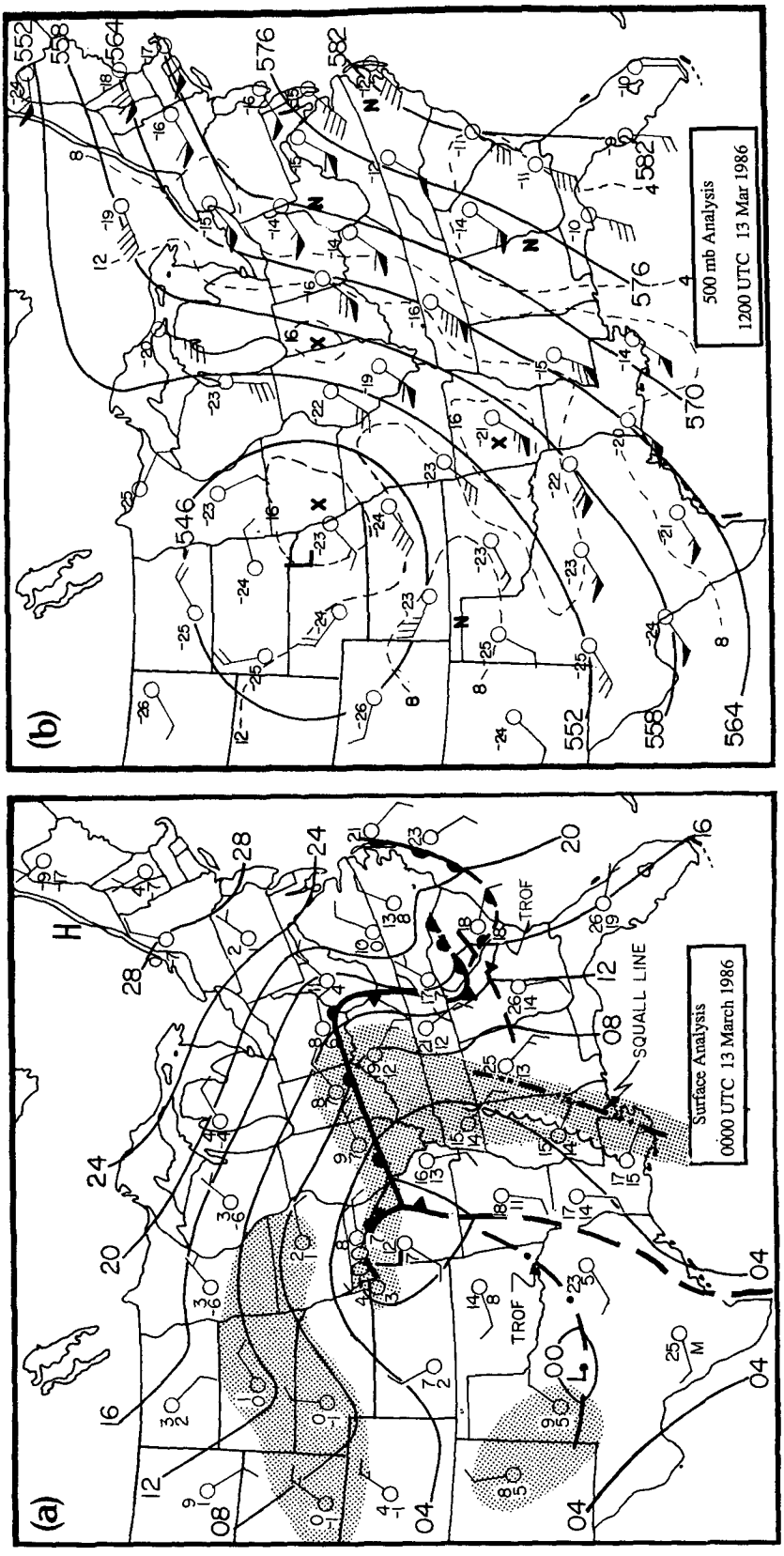


FIG. 4. (a) Sea-level pressure analysis for 13 March 1986 0000 UTC. Solid contours are isobars (12 = 1012 mb). Fronts indicated with the usual symbols. Frontogenesis indicated by dashed line with pips on every dash. Dash–dot line shows the position of the arctic front. Dash–double-dot line shows the position of the squall line, and the scalloped line marks the leading edge of cold advection at 700 mb (CFA). Station reports show wind velocity (½ barb = 2.5 m s$^{-1}$, barb = 5 m s$^{-1}$), temperature, and dewpoint (°C). Shading indicates regions of general precipitation. (b) Analysis of 500-mb heights (solid contours every 60 m) and absolute vorticity ($10^{-5}$ s$^{-1}$) for 0000 UTC 13 March 1986. The symbol × denotes vorticity maxima and *N* denotes vorticity minima. Station reports include wind velocity (barb = 5 m s$^{-1}$, flag = 25 m s$^{-1}$) and temperature (°C).


FIG. 5. GOES infrared satellite image for 0000 UTC 13 March 1986. The dashed line indicates the position of a dry line. The scalloped line marks the estimated leading edge of cold advection at 700 mb (CFA).

section analysis reveals a transition zone that separates advancing cold air from warm air in the middle troposphere to the east of the surface trough. The leading edge of the zone of transition is located west of Centreville, Alabama (CKL), along the leading edge of the 700-mb cold-air advection at this time (Fig. 6a). Hobbs et al. (1990) refer to this feature as a cold front aloft (CFA). The authors use this term to denote cold-frontal zones whose bases are above the surface in the lower or middle troposphere, and note that in some cases the CFA may have its origin as an upper-level front, of the type discussed by Reed (1955) and Keyser and Shapiro (1986). Petterssen (1956) suggested that features like a CFA might be produced when a maritime cold front passes over the Rocky Mountains and encounters potentially denser air to the east, forcing the frontal zone aloft. Martin et al. (1989) document a CFA that was produced in an analogous manner in another GALE case study. They show a significant increase in the intensity of precipitation along a coastal front over the Carolinas when it is overtaken by the CFA. The analysis of a CFA in the present case provides a conceptual aid for diagnosing measurable weather in the absence of apparent frontal structure at the surface.

Evidence for the presence of a CFA in this case can be seen in the temperature analysis and in the pattern of cold advection (evidenced by backing of the wind with height) aloft over Little Rock, Arkansas (LIT), east of the position of the surface trough (Fig. 7a). It is beyond the scope of this paper to fully document the origin of the CFA in this case. However, evidence suggests that the air behind the CFA had its origin at or near the tropopause, consistent with the results of earlier investigations of upper-level cold fronts (e.g., Reed and Sanders 1953; Keyser and Shapiro 1986). Analysis of potential vorticity (Ertel 1942), a conservative tracer for adiabatic motions in the atmosphere, gives some insight into the origin of the air behind the CFA. Potential vorticity combines absolute vorticity and vertical stability [$P = (\zeta_\theta + f)\partial\theta/\partial p$ where, $\zeta_\theta$ is the relative vorticity on isentropic surfaces, $\theta$ is potential temperature, and $p$ is pressure], and has been used to show that upper-level fronts contain air of stratospheric origin (e.g., Reed 1955). Hobbs et al. (1990) calculated potential vorticity for 0000 UTC 13 March using the NGM C grid initialized data from NMC. The increase in potential vorticity across the CFA (Fig. 7a) indicates that the air behind the CFA may indeed have had its origin in the upper troposphere. Equivalent potential temperature and relative humidity fields (Fig. 7b) indicate that the air behind the CFA is significantly drier than ahead. The analyzed position of the CFA is indicated by a scalloped line in Fig. 4a. Evidence will be presented in sections 6 and 7 that implicates thermal-

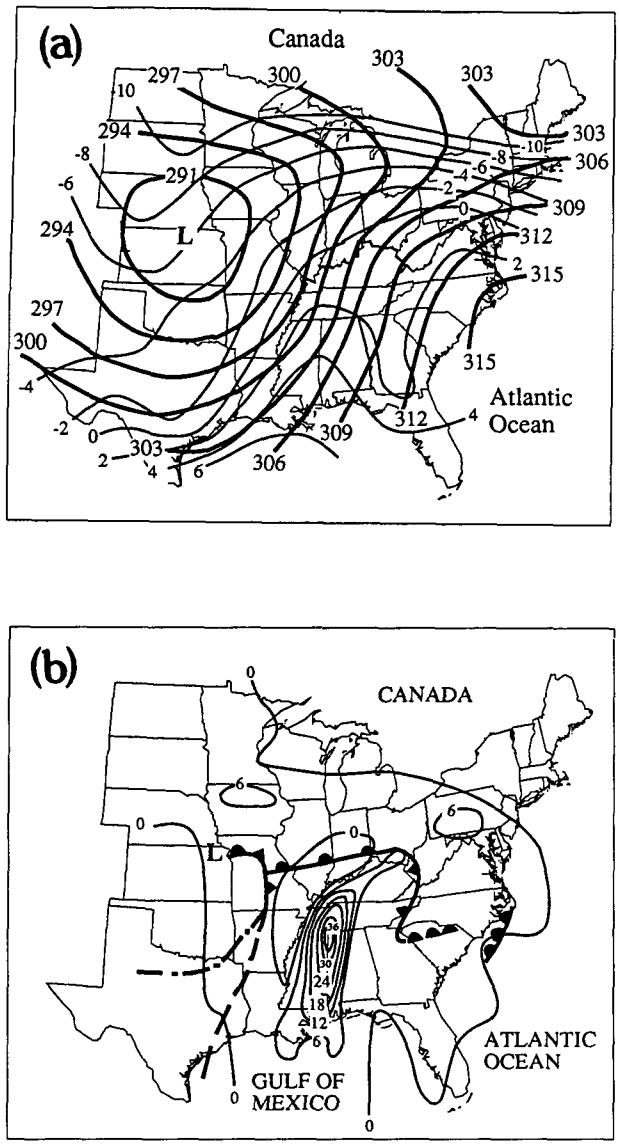


FIG. 6. (a) Analysis of 700-mb heights (bold contours every 30 m) and temperature (thin contours every 2°C) for 13 March 1986 at 0000 UTC. (b) The 12-h forecast of 700-mb vertical velocity for 0000 UTC 13 March 1986 from the NMC's nested grid model (contours every 1 cm $s^{-1}$).

advection patterns associated with the CFA in the formation of the squall line along the Piedmont front over North Carolina.

The surface analysis for 1200 UTC 13 March (Fig. 8a) shows high pressure over Maine and eastern Canada continuing to force cold air southward along the eastern slopes of the Appalachians. The surface low is centered over southern Iowa with a warm front extending eastward into the Ohio Valley where it becomes stationary along the western slopes of the Appalachians. The front continues around the southern Appalachians into Georgia in response to the cold-air damming. Frontogenesis is continuing inland along the margin of the Carolina Piedmont, while the coastal front, which was off the Carolina coast at 0000 UTC, is undergoing frontolysis as it moves over cool nearshore waters along the Carolina coast. The squall line extending from southern Alabama into north-central Georgia at this time (Fig. 8a) lies just to the east of the leading edge of cold advection at 700 mb (not shown) associated with the CFA. The 500-mb height and vorticity analysis for 1200 UTC 13 March 1986 (Fig. 8b) shows a closed low still centered over Nebraska with a jet streak (40 m $s^{-1}$) crossing Tennessee. Cold advection is implied over western North Carolina at this time, and the minimum in absolute vorticity at 500 mb continues over the inner GALE area.

Cross-section analysis for 1200 UTC (Fig. 9) reveals a pattern similar to that seen at 0000 UTC (Fig. 7), with cold-air advection continuing over Little Rock, Arkansas (LIT) and cooler air approaching Nashville, Tennessee (BNA) at mid-tropospheric levels (Fig. 9a) associated with the CFA. Relative humidity analysis at this time shows marked dry air between ~700 and 400 mb over BNA (Fig. 9b). Equivalent potential temperature decreases with height above LSF and AYS indicating a substantial layer unstable to moist convection if sufficiently lifted. Southwesterly flow of dry air aloft (RH < 50% from ~550 to 400 mb) over a layer of moist air (RH > 90%) in the lower troposphere at LSF, provides conditions conducive to the development of deep convection (Fawbush et al. 1951; Bosart 1973) in the vicinity of the squall line.

## 4. Mesoscale analyses

To investigate in more detail the formation of the Piedmont front, mesoscale analyses were constructed and parcel-following frontogenesis was calculated using all available surface data, including data from PAM II stations, NWS stations, buoys, and ships of opportunity.

The intensity of surface frontogenesis is defined as the individual rate of increase of the gradient of a scalar property $S$ that has a continuous distribution in the horizontal $(x, y)$ plane (Petterssen 1956 and Miller 1948). Neglecting diabatic effects, the total adiabatic frontogenesis following a parcel can be written (after Petterssen 1956):

$$F_2 = \frac{d|\nabla_2\theta|}{dt} = -\frac{\partial\theta/\partial x}{|\nabla_2\theta|}\left(\frac{\partial u}{\partial x}\frac{\partial\theta}{\partial x} - \frac{\partial v}{\partial x}\frac{\partial\theta}{\partial y}\right) - \frac{\partial\theta/\partial y}{|\nabla_2\theta|}\left(\frac{\partial v}{\partial y}\frac{\partial\theta}{\partial y} - \frac{\partial u}{\partial y}\frac{\partial\theta}{\partial x}\right).$$

An objective analysis scheme was employed to interpolate data to a regular gridpoint array (with a grid spacing of 34 km) for the purpose of making finite-difference calculations. The Barnes (1964, 1973) objective analysis method was utilized for this purpose

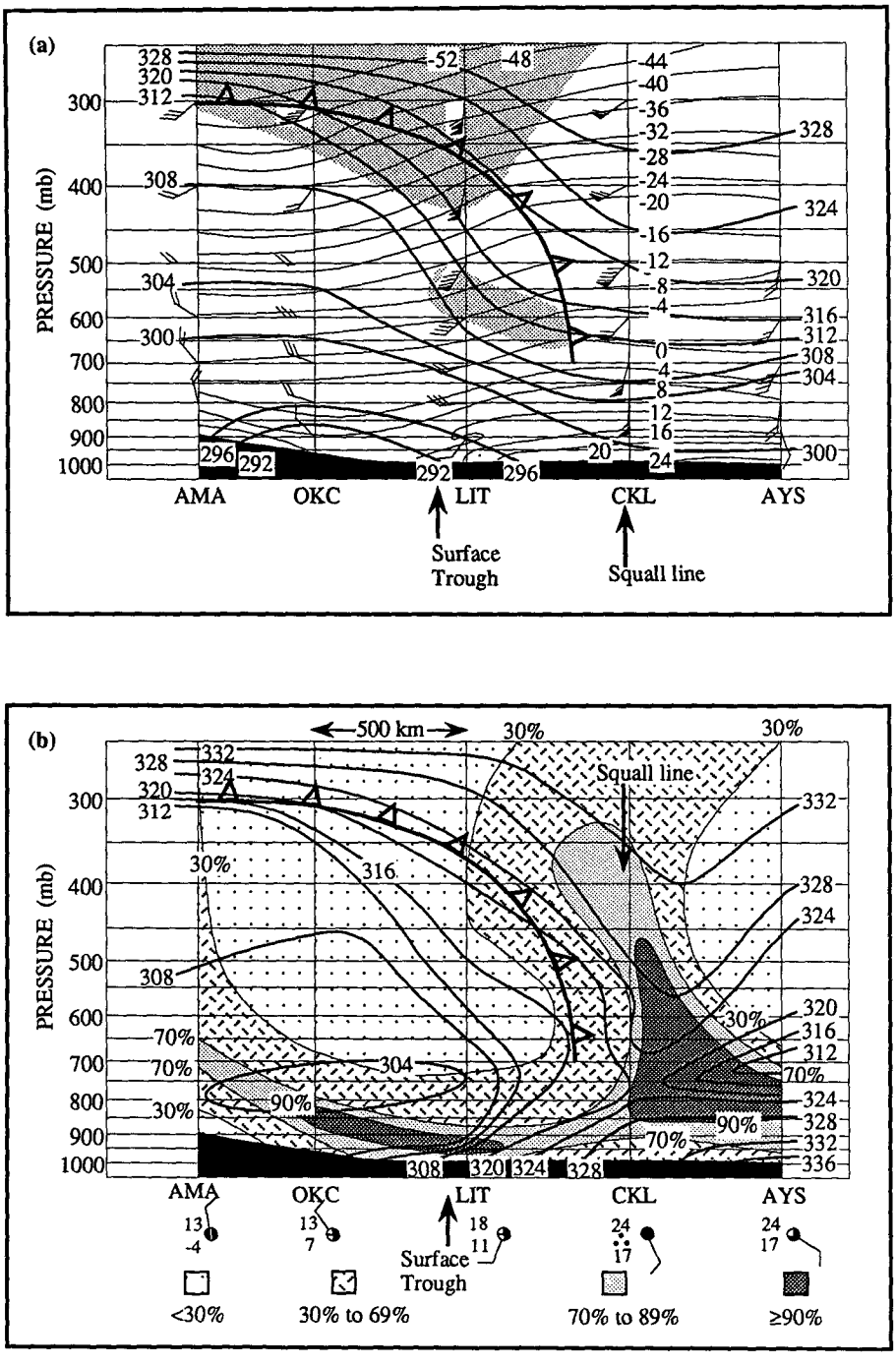


FIG. 7. Cross section between Amarillo, Texas (AMA), and Waycross, Georgia (AYS), for 0000 UTC 13 March 1986 (see heavy solid line in Fig. 8b). Heavy solid line with open cold front symbols indicates the approximate position of the CFA. (a) Thin solid contours are potential temperature (K). Dashed contours are temperature (°C). Rawinsonde winds plotted with the usual convention (flag = 25 m $s^{-1}$, barb = 5 m $s^{-1}$, ½ barb = 2.5 m $s^{-1}$). Shading indicates region in which the potential vorticity is ≥1 × $10^{-6}$ K m s $kg^{-1}$ (after Hobbs et al. 1990). (b) Solid contours are equivalent potential temperature (K) and shading pattern indicates relative humidity. Current surface weather is displayed at the bottom of the figure for each sounding station.

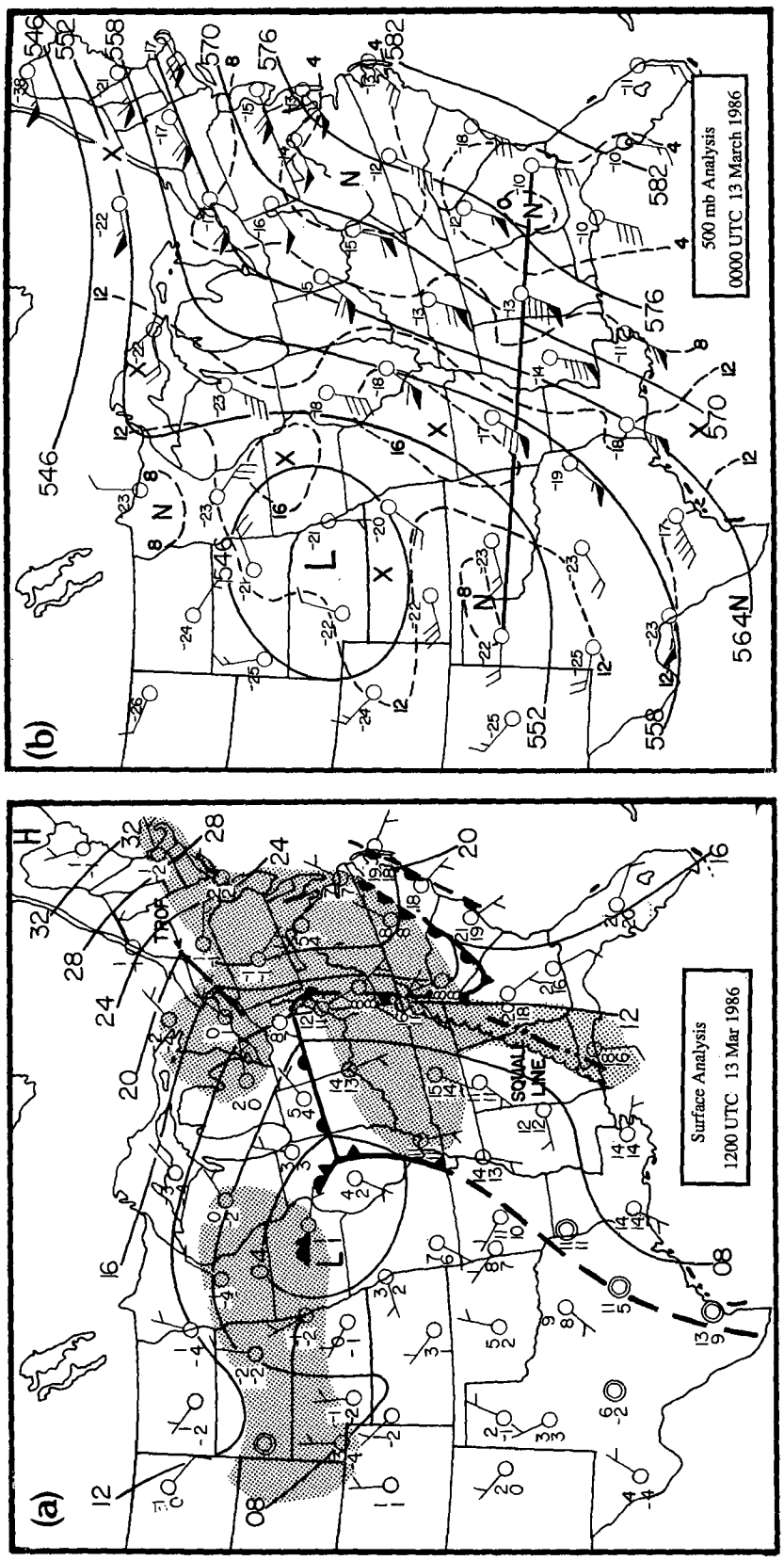


FIG. 8. Same as Fig. 4 for 1200 UTC 13 March 1986. The heavy solid line in (b) indicates the approximate location of the cross sections shown in Figs. 7 and 9.

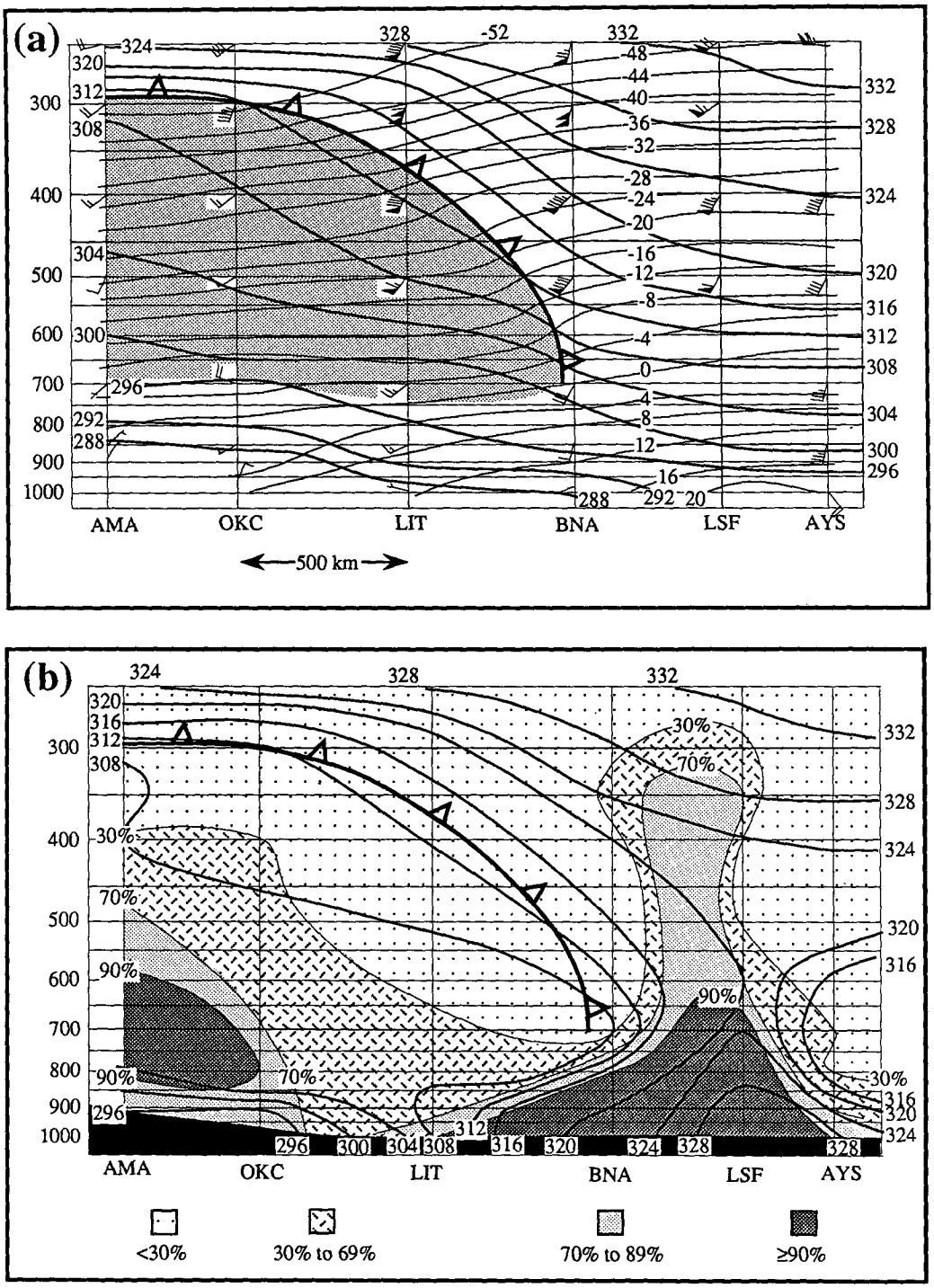


FIG. 9. Cross section from Amarillo, Texas (AMA), to Waycross, Georgia (AYS), for 1200 UTC 13 March 1986. Heavy solid line with open cold front symbols indicates the approximate position of the CFA. (a) Thick solid contours are potential temperature (K), and thin contours are temperature (°C). Rawinsonde winds plotted with the usual convention (flag = 25 m $s^{-1}$, barb = 5 m $s^{-1}$, ½ barb = 2.5 m $s^{-1}$). Shading indicates region in which the winds back with height. (b) Solid contours are equivalent potential temperature (K) and shading pattern indicates relative humidity. Refer to Fig. 8b for location of cross section.

(see the Appendix). The results are presented in a series of surface analyses (Figs. 10–15) that depict the evolution of the Piedmont front from the time that frontogenesis was first detected over the inner GALE area (0000 UTC 13 March), to the time of squall line development over North Carolina (2100 UTC 13 March).

The surface analysis at 0000 UTC 13 March (Fig. 10a) shows the wedge of cold air and associated surface pressure ridge to the east of the Appalachians. A coastal front that developed in the vicinity of the Gulf Stream front during the previous ~12 h can be seen off the Carolina coast as a warm front. Cloudy skies prevail throughout the inner GALE area with a few showers and drizzle in South Carolina. A weak temperature gradient can be seen in the PAM-II data across the southeast portion of the inner GALE area (Fig. 10b). Streamline analysis shows confluence over South Carolina leading to the frontogenesis (Fig. 10c). Since the thermal gradient is relatively weak, the magnitude of the total frontogenesis is small at this time. Offshore data imply that the coastal front may also be experiencing frontogenesis at this time. However, this is not confirmed by the frontogenesis calculations since it lies outside the objective analysis grid, which stops over the nearshore waters (see Fig. 3b).

At 0600 UTC 13 March the surface analysis (Fig. 11) shows that an enhanced thermal gradient has formed over South Carolina (Fig. 11b), consistent with frontogenesis over that area at 0000 UTC. The initial section of the developing Piedmont front is analyzed as a stationary front over South Carolina at this time (Fig. 11a). Widespread fog has developed on both sides of the front with light rain, drizzle, and showers prevalent in the cold air farther north. At this time, streamline analysis reveals increasing confluence over southeastern North Carolina (Fig. 11b). The line of confluence over North Carolina is a northeastward extension of the confluence line over South Carolina. The thermal gradient over North Carolina is weaker than the gradient observed over western South Carolina at this time (Fig. 11b). Figure 11c shows a broad, but weak area of frontogenesis over the Carolinas. Offshore data imply that frontogenesis is continuing to occur along the northern end of the coastal front (Fig. 11a).

By 1200 UTC the surface analysis (Fig. 12) indicates that the axis of confluence has continued to form northeastward over central North Carolina, with cold-air damming still evident north of this line. Drizzle, light rain, and fog northwest of the Piedmont front and partly cloudy conditions south of the Piedmont front over South Carolina are resulting in a gradient of surface diabatic heating across the front beginning at this time (Fig. 12a). (Calculations of the magnitude of this heating were not attempted due to insufficient data on soil temperature and moisture and vegetation distribution.) The Piedmont front over South Carolina has strengthened (Fig. 12b), as evidenced by the enhanced

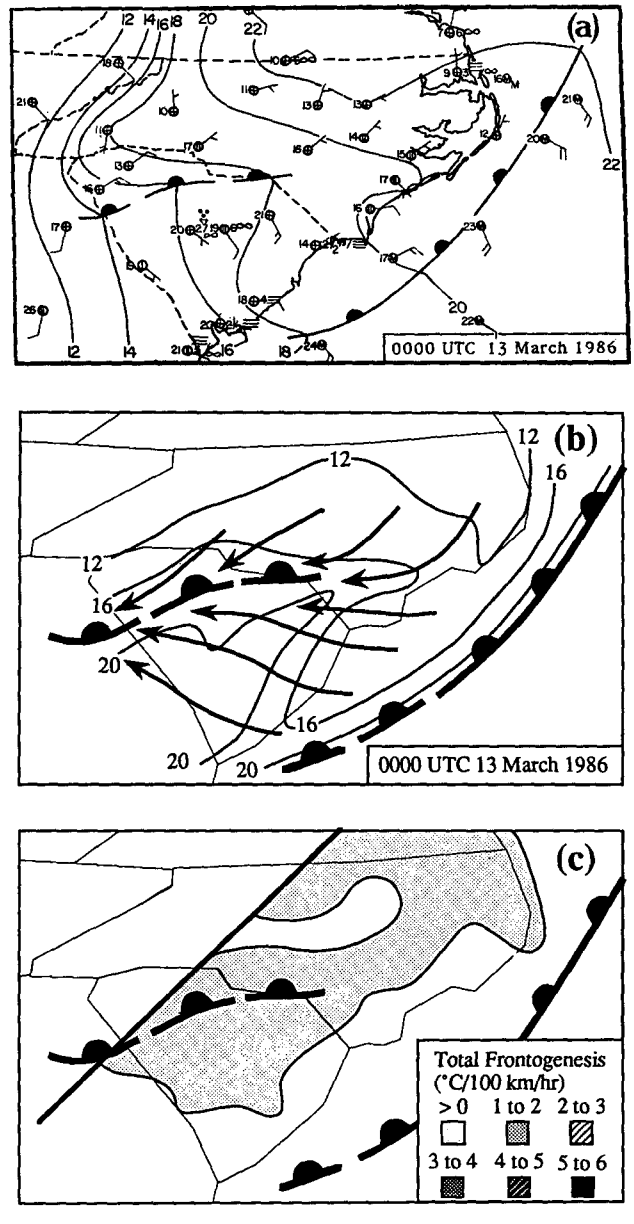


FIG. 10. Mesoscale analysis for 0000 UTC 13 March 1986. Frontal positions are shown with the usual convention. Frontogenesis lines are indicated by dashed lines with pips on every dash. (a) Sea-level pressure analysis (solid contours are isobars every 2 mb), with NWS and FAA station reports of wind velocity (½ barb = 2.5 m $s^{-1}$, barb = 5 m $s^{-1}$), temperature (°C), current weather, and sky conditions. (b) Isotherm analysis (thin solid contours every 2°C) and streamline analysis. (c) Total frontogenesis [°C(100 km $h^{-1}$)$^{-1}$]. The heavy straight line marks the western boundary of the calculations.

thermal gradient over this area. Relatively weak thermal gradients are seen over North Carolina. Streamlines, however, indicate confluence along the extent of the incipient front. Total frontogenesis calculations (Fig. 12c) indicate that the Piedmont front was strengthening most rapidly over central South Carolina,

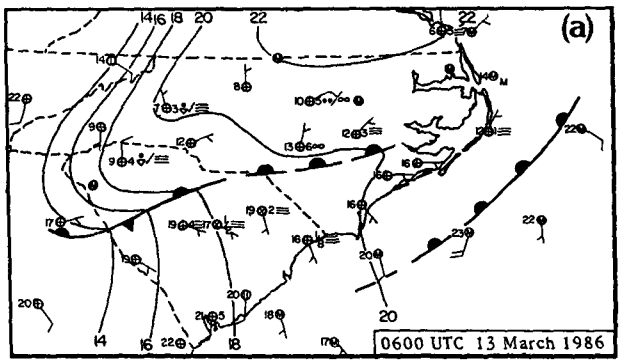


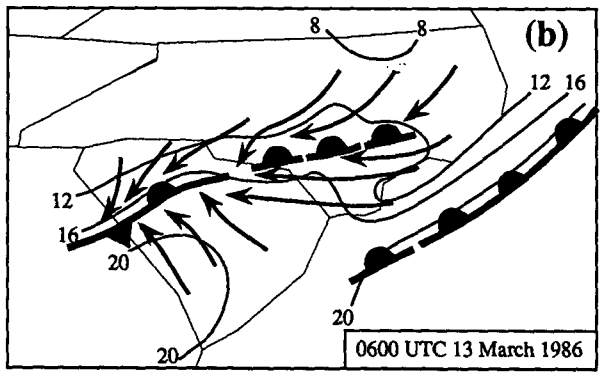


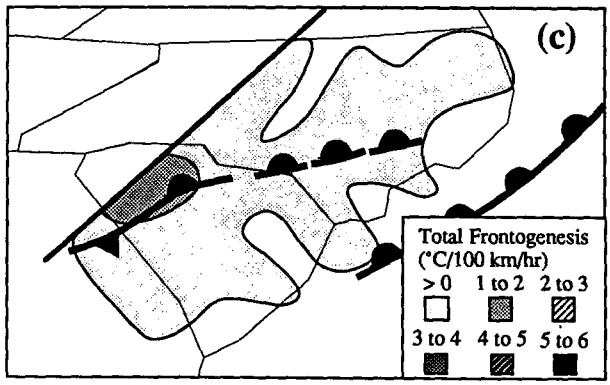


FIG. 11. Same as Fig. 10 for 0600 UTC 13 March 1986.

consistent with the continuing confluence observed in the presence of a strengthening temperature gradient. Analysis indicates that the coastal front is dissipating over the nearshore waters at this time.

Three hours later at 1500 UTC a continuous Piedmont front is analyzed from northwest South Carolina across northeast North Carolina (Fig. 13a). The cold-air damming, evidenced by the surface pressure ridge, is prevailing north of the front at this time. North of the front in central and western North Carolina the winds are generally north or northeast and the weather consists of light rain, drizzle, and fog with overcast or obscured skies. South of the front surface temperatures continue to rise under variable cloudy skies. A strong thermal contrast has developed along the Piedmont front (Fig. 13b). It is clear that solar insolation has played a major role in the change in the temperature field to the south of the Piedmont front from 1200 to 1500 UTC. The streamline analysis (Fig. 13b) shows 180° wind shifts across the front near south central North Carolina and 90° wind shifts across the front over the remainder of eastern North Carolina. Frontogenesis (Fig. 13c) is strongest in the vicinity of the largest wind shift. In comparing the observed winds

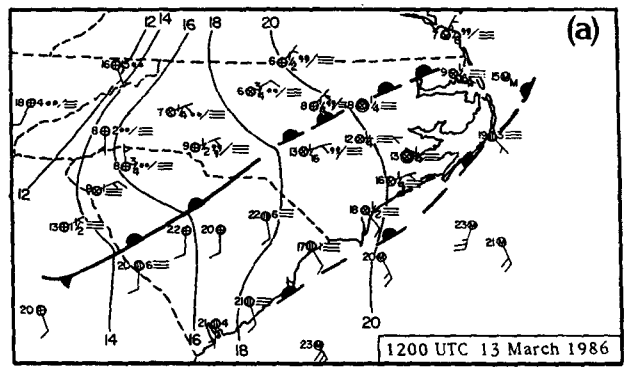


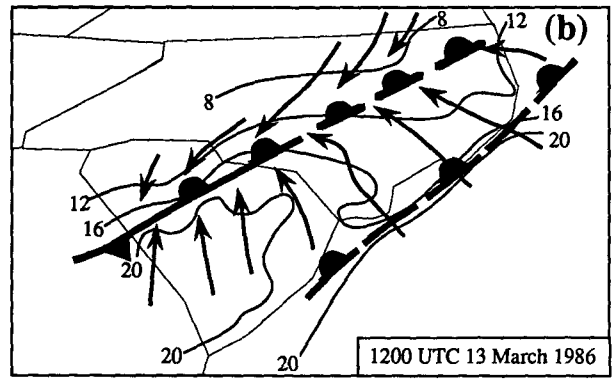


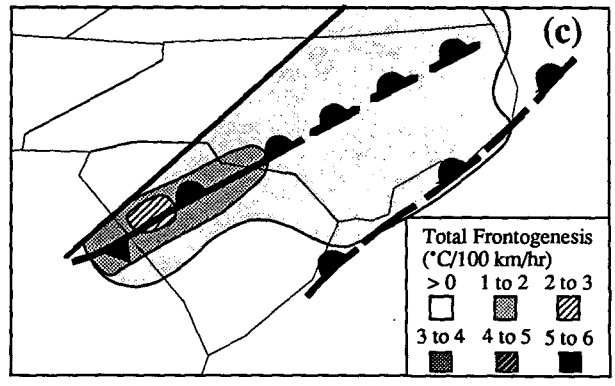


FIG. 12. Same as Fig. 10 for 1200 UTC 13 March 1986.

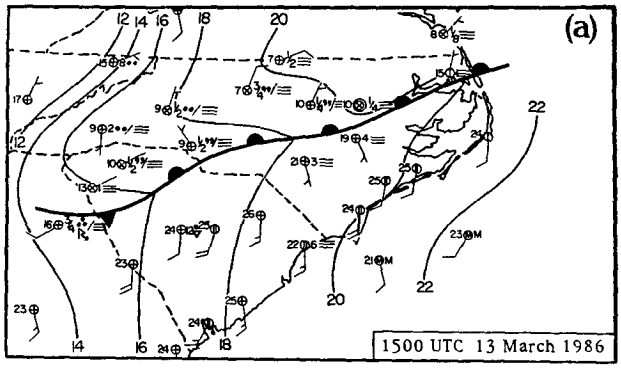


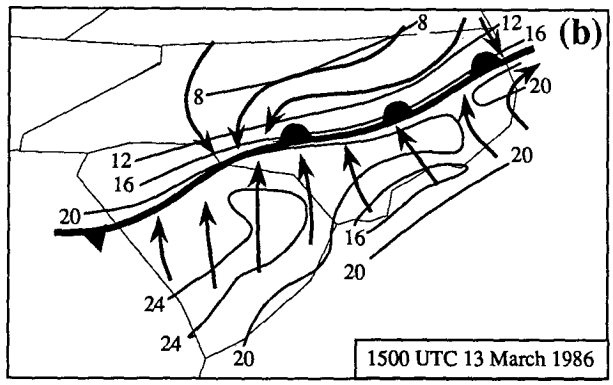


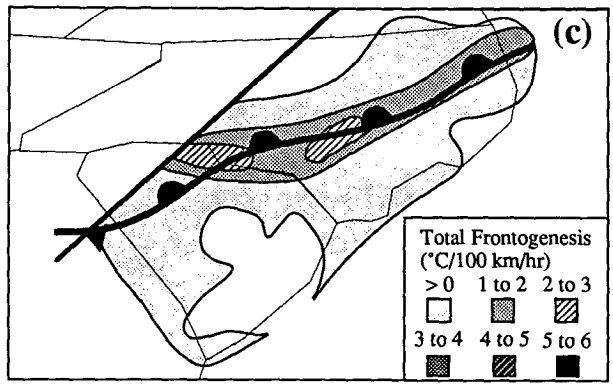


FIG. 13. Same as Fig. 10 for 1500 UTC 13 March 1986.

and the isobar pattern (Fig. 13a) it is apparent that the frontogenesis (Fig. 13c) is present in the observed winds, but is much weaker in the geostrophic winds. It is over this region where the first of a series of mesolows forms over North Carolina.

By 1800 UTC, a mesolow has formed over central North Carolina (Fig. 14a). Wind shifts observed in the vicinity of the Georgia–South Carolina border between 1500 and 1800 UTC are in response to a second weaker mesolow moving in from the west. PAM-II winds proved to be an important tool in refining the location of the mesolows documented in this paper. Streamlines (Fig. 14b) show flow converging into the mesolow. Continued strengthening of the Piedmont front is evidenced by the magnitudes of the thermal gradient and frontogenesis (Figs. 14b,c). The western part of the Piedmont front over South Carolina has begun to move southeast at this time.

The final mesoscale analysis in this series at 2100 UTC shows two mesolows that are slowly tracking east-northeast (Fig. 15a). Although streamline analysis continues to show confluence, the temperature gradient

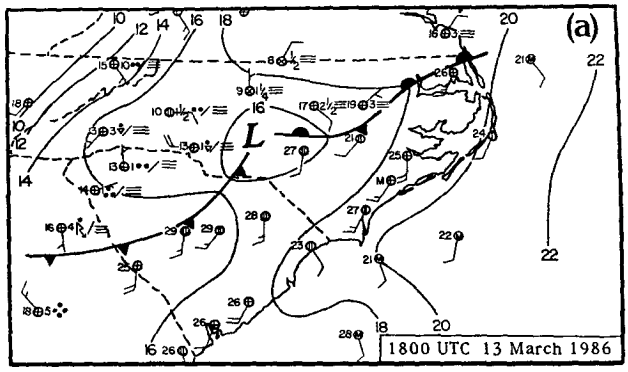


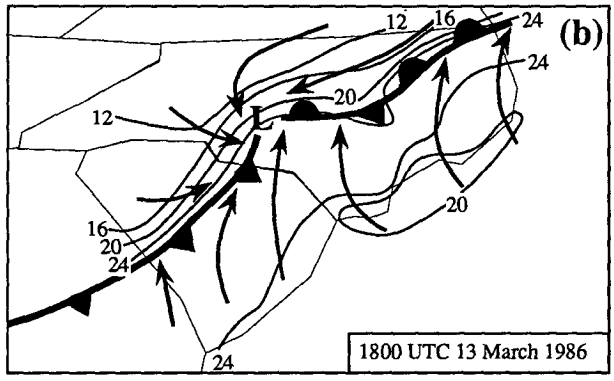


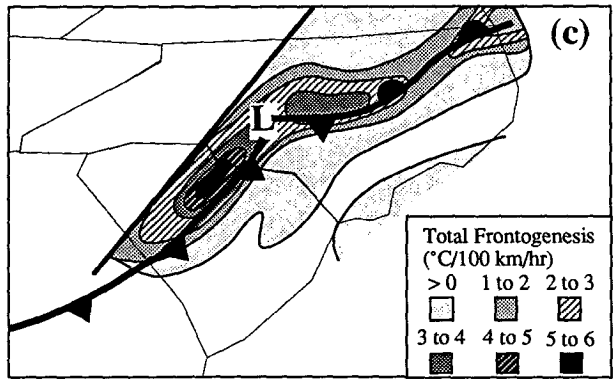


FIG. 14. Same as Fig. 10 for 1800 UTC 13 March 1986.

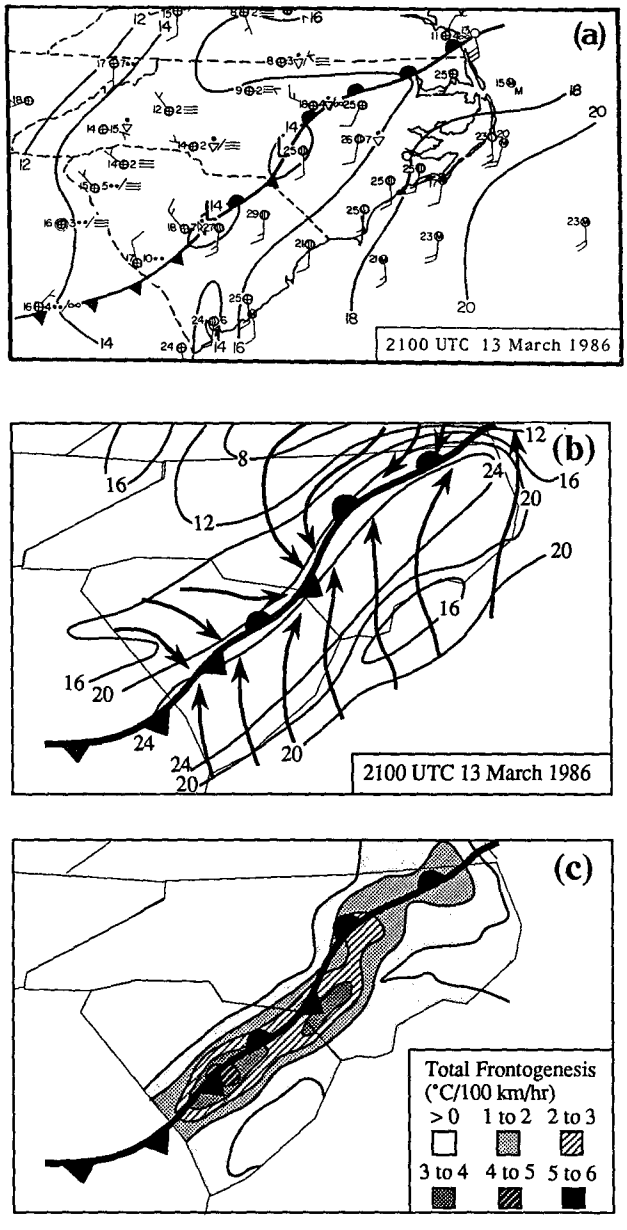


FIG. 15. Same as Fig. 10 for 2100 UTC 13 March 1986.

has not strengthened significantly along the Piedmont front in the intervening 3 h since 1800 UTC (Fig. 15b). Four severe thunderstorms have been reported over the Carolinas between 1800 and 2100 UTC. A squall line is forming along the Piedmont front in the region of enhanced frontogenesis extending from northern South Carolina to central North Carolina (Fig. 15c). Details of these developments are the subject of the next section.

## 5. Severe weather development

Satellite, radar, and rawinsonde observations will be utilized in this section to document the development of convective instability and severe weather over the Carolinas, and the initiation of a convective line along the Piedmont front.

Six digitized NWS radars (Bristol, Tennessee; Volens, Virginia; Cape Hatteras, North Carolina; Wilmington, North Carolina; Charleston, South Carolina; and Athens, Georgia), with 250-km scan radii provided complete data coverage of the inner GALE area. Radar summary charts (Fig. 16) displaying radar reflectivity (D/VIP levels, see Table 1) and echo-top heights were adapted from NWS summary charts and digitized radar mosaics.

The radar summary for 1535 UTC (Fig. 16a) depicts a small area of showers and thunderstorms that developed over eastern South Carolina around 1500 UTC. Light overrunning precipitation is evident over northwestern North Carolina. This light stratiform precipitation was present as early as 0600 UTC and persisted north of the Piedmont front through 1800 UTC, just prior to severe weather development. The northern end of a squall line can be seen over western South Carolina which continues through Georgia, Alabama, and Florida. The history of this squall line is seen in Figs. 4a and 8a. The northern end of this squall line merges with the convective line that forms farther east over South and North Carolina by 2200 UTC (Fig. 16e), while the southern portion over Georgia gradually dissipates.

From 1530 to 1830 UTC the Piedmont front remained quasi-stationary and the area of convective showers and thunderstorms that initially developed over South Carolina extended northeastward in a band oriented nearly parallel to the Piedmont front (Figs. 16a,b). By 1830 UTC a mesolow ($L_1$) had formed over central North Carolina, just west of the developing convection (see Figs. 14a and 16b). In association with the development of mesolow $L_1$, the western part of the Piedmont front has started to move southeastward.

Figure 17 shows a cross section from BNA to the research vessel *Cape Hatteras* (RVC) that crosses the squall line just east of AHN (see Fig. 3a) and the southern end of the Piedmont front over South Carolina at 1800 UTC 13 March 1986. At this time backing of the winds with height at midlevels over AHN and noticeable cooling at ~700 mb (Fig. 17a) provide evidence of the presence of the CFA. Further west, BNA shows dry conditions at all levels above the surface (Fig. 17b). East of AHN equivalent potential temperatures decrease with height from the surface to ~650 mb, reflecting the relative humidity pattern. Relative humidities are high below ~800 mb with relatively dry air above ~650 mb, resulting in conditions conducive to deep convection. Over AHN, the relative humidity is high (>90%) from the surface to 550 mb, in the wake of the squall line over Georgia and South Carolina at this time (see Fig. 16b).

GOES visible satellite imagery for 1830 UTC 13 March 1986 (Fig. 18a) shows convective cells in the

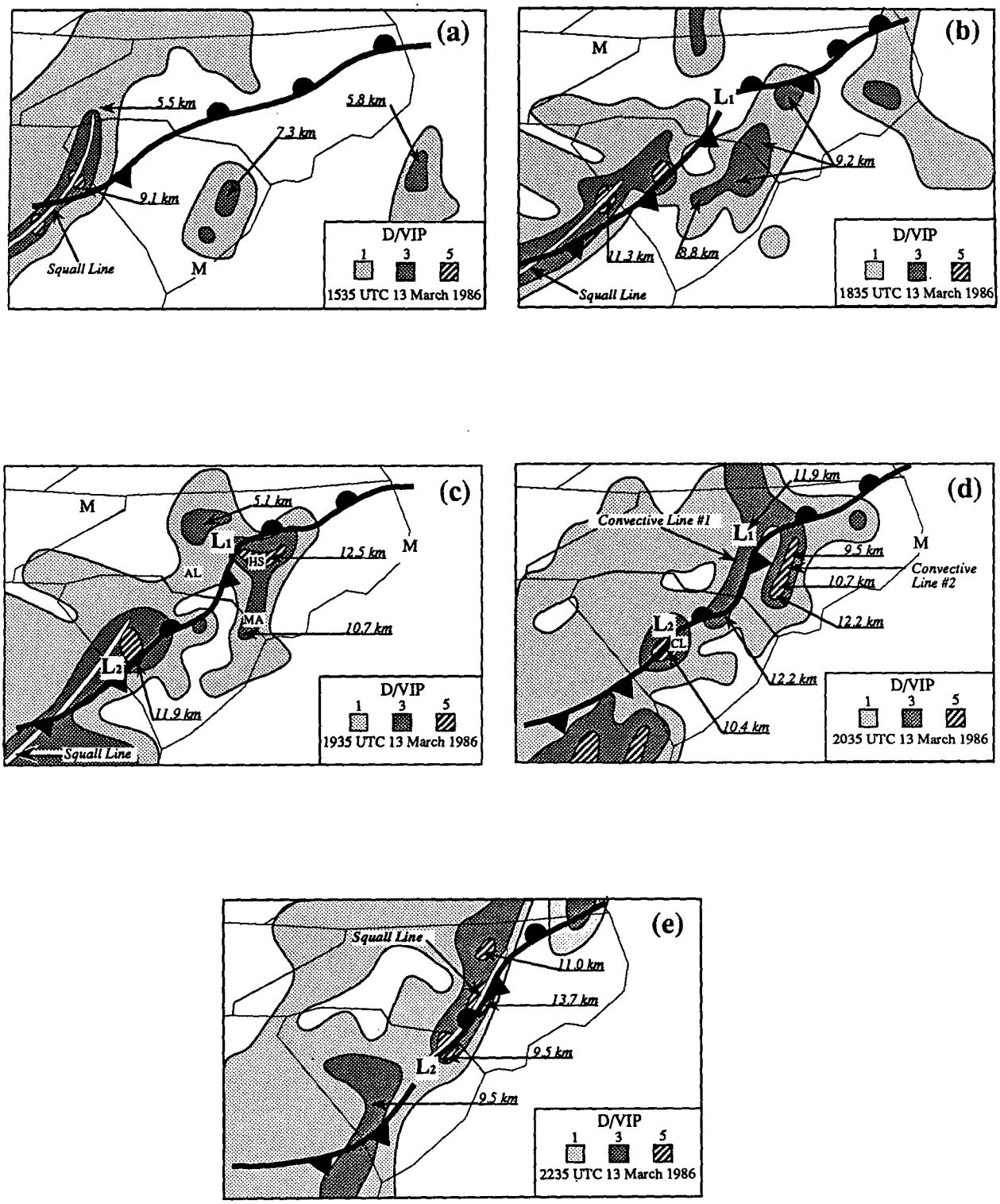


FIG. 16. Radar summaries for 13 March 1986, with D/VIP levels shaded and height of maximum precipitation tops indicated. (a) Radar summary for 1535 UTC, (b) radar summary for 1835 UTC, (c) radar summary for 1935 UTC. AL, MA, and HS indicate the locations of Albemarle, Marietta, and Holly Springs, North Carolina, respectively, (d) radar summary for 2035 UTC. CL indicates the location of Columbia, South Carolina, (e) radar summary for 2235 UTC. "M" indicates radar site was not operating at this time. Frontal positions are for the half-hour (5 min preceding the radar times).

TABLE 1. Relationship between VIP level and reflectivity intensity, estimated precipitation, and rainfall rate for stratified and convective clouds. Rainfall rates given in millimeters per hour (from Federal Meteorological Handbook #7 1981).

| VIP level | Reflectivity (dBZ) | Estimated precipitation | Rainfall rate (mm $h^{-1}$) | |
|---|---|---|---|---|
| | | | Stratiform | Convective |
| 1 | <30 | Light | <2.5 | <5.1 |
| 3 | 40–46 | Heavy | 2.5 to 13 | 5 to 28 |
| 5 | 50–55 | Intense | N/A | 114 to 180 |

warm moist air over east-central North Carolina (arrow A in Fig. 18a). A suppression of cumulus can be seen in the subsidence region to the west of these cells in the vicinity of the surface mesolow (arrow B in Fig. 18a). Cloud streets of shallow convection are visible in the warm sector. This shallow convection acts to destabilize the atmosphere by moistening and warming the lower cloud layer, with cooling occurring above (Betts 1973). Air that has been so modified can be more easily forced to deep convection (Purdom 1979). A second area of convective clouds is developing north of the Piedmont front over central North Carolina (arrow C, Fig. 18a), and is associated with the area of precipitation seen northeast of the Piedmont front in Fig. 16b. It is suggested that this convection is forming along the leading edge of the CFA over North Carolina at this time.

Strong straight-line winds (>25 m $s^{-1}$) ripped a roof off of a building in Albemarle, North Carolina, at ~1900 UTC (AL in Fig. 16c) and were attributed to the passage of a severe thunderstorm (NOAA 1986). This storm developed in an area of maximum frontogenesis (Fig. 14c), moisture-flux convergence, and upward vertical velocity (the latter two will be discussed in detail later in this paper) associated with the Piedmont front and mesolow $L_1$. Radar data, including digital PPIs, however, show little in the way of precipitation echo in this area at 1835 UTC (Fig. 16b).

At 1935 UTC, NWS digital radar data shows two areas of convective precipitation over North Carolina. The NWS radar summary for this time is given in Fig. 16c. A second mesolow ($L_2$) has developed over Georgia and is located over the South Carolina–Georgia border at 1930 UTC. During the hour following 1930 UTC three additional severe thunderstorms were observed: at Marietta, North Carolina, damage from large hail was reported at ~1955 UTC; at Holly Springs, North Carolina, strong straight-line winds downed trees at ~2000 UTC, and at Columbia, South Carolina, wind and hail damage were reported at ~2015 UTC. All four of the severe thunderstorms discussed in this section occurred in regions of enhanced moisture-flux convergence, and followed the time of maximum frontogenesis along the Piedmont front (Fig. 14c). In the case of the Columbia storm enhanced moisture-flux convergence was associated with mesolow $L_2$. The maximum echo tops in the vicinity of Holly Springs, North Carolina, increased from 9.2 to 12.5 km between 1835 and 1935 UTC, the most rapid increase observed. Maximum tops in the area of precipitation north of the Piedmont front are 5.1 km (~550 mb).

The visible satellite image for 1930 UTC shows a line of cloud oriented north–south (arrow A, Fig. 18b) associated with the convective precipitation observed just east of the Piedmont front (Fig. 16c). The severe thunderstorms at Marietta and Holly Springs developed in this line. The cloud-free area to the west of the convective line has become better defined with time. The development of the line of convection occurred coincident with the maximum frontogenesis along the Piedmont front (Fig. 14c), probably a reflection of the fact that solar radiation has resulted in the greatest warming of the surface air in the warm sector, maximizing the gradient across the front, and the buoyancy of the warm sector air. The convective line and clear zone both occur to the east of the surface front. A second line of convection developing northwest of the Piedmont front can be seen in central North Carolina at this time (arrow B, Fig. 18b). This convective line is an outgrowth of the convective activity seen earlier (Fig. 18a), and is occurring in the unstable air above the Piedmont front, and as will be shown later in this paper is associated with synoptic forcing ahead of the CFA (Fig. 17).

During the following hour the second convective line overtakes the Piedmont front, and the maximum height of echoes increases to 12.2 km (Fig. 16d), the same as that observed for the thunderstorms along the first convective line at this time. The 2100 UTC infrared satellite image (Fig. 18c) supports the presence of two separate convective lines with cloud-top temperatures ~ −45°C. It is suggested that subsynoptic-scale lifting associated with the CFA contributes to the formation of the second (more westward) line of convection.

A traverse through the two convective lines and front was made by instrumented car (Fig. 19). The GALE chase team started ~65 km southeast of Raleigh, North Carolina, on U.S. Route 70 at 1850 UTC (corresponding to the right side of Fig. 19). Towering cumulus could be seen to the west-northwest at this time, and the temperature was ~23°C. Traveling northwest towards Raleigh, the temperature remained approximately constant at ~23°C, indicative of the warm air south of the Piedmont front. At ~1930 UTC the chase team was located just south of the Raleigh–Durham weather station (RDU) as it passed through the northern end of the first convective line. RDU was reporting a thunderstorm at this time. Cooler air associated with the downdrafts of thunderstorm cells in this line caused temperatures to begin dropping as the chase team continued northwest toward Durham, North Carolina. The Piedmont front, accompanied by rain and gusty winds, was encountered at 2004 UTC ~16 km west of Dur-

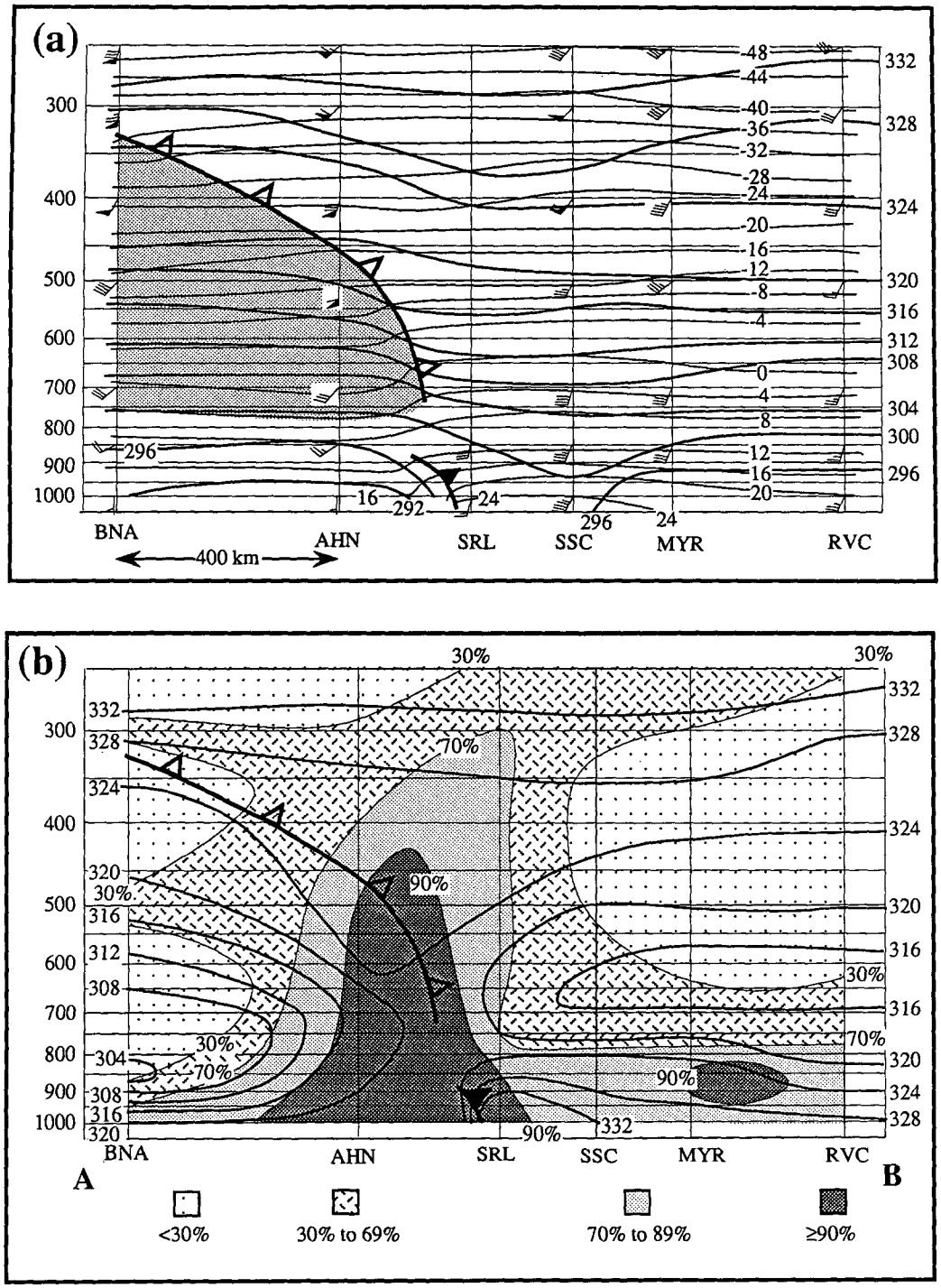


FIG. 17. Same as Fig. 9 for 1800 UTC 13 March 1986 for cross section AB from Nashville, Tennessee (BNA), to the research vessel *Cape Hatteras* (RVC). Refer to Fig. 3a for location.

ham on Interstate 40. A sharp temperature gradient associated with this feature is evident (Fig. 19).

As the Piedmont front and second convective line continue to advance, the two convective lines merge to form a squall line, with a narrow band of heavy precipitation (up to ~180 mm $h^{-1}$) in the digital radar data by 2200 UTC. Precipitation echoes are detected up to 13.7 km along the squall line, the maximum height observed during this case study (Fig. 16e). After 2300 UTC as night approaches, the squall line weakens

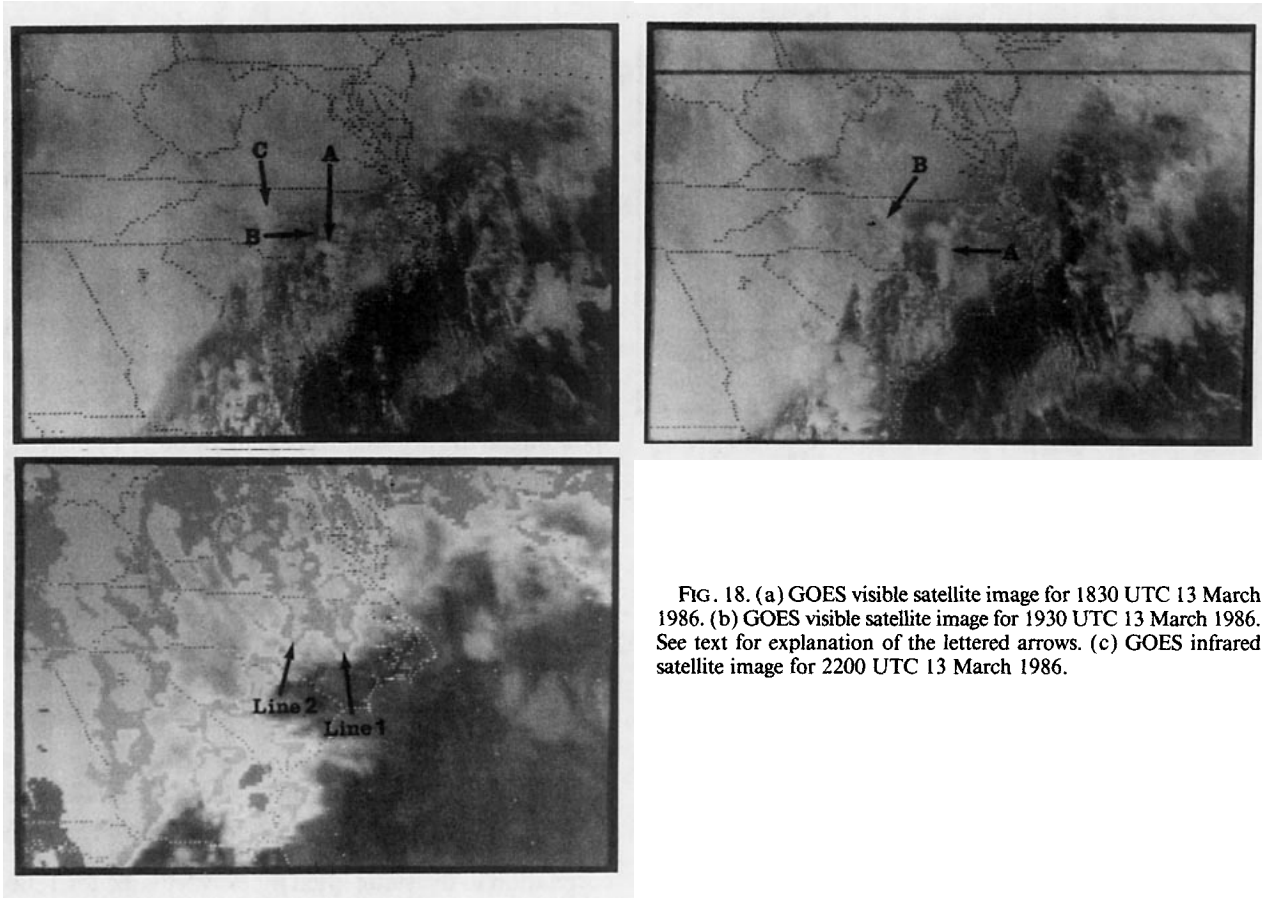


FIG. 18. (a) GOES visible satellite image for 1830 UTC 13 March 1986. (b) GOES visible satellite image for 1930 UTC 13 March 1986. See text for explanation of the lettered arrows. (c) GOES infrared satellite image for 2200 UTC 13 March 1986.

as it crosses the coastal plain, and approaches the cool nearshore waters.

## 6. Stability analysis

In this section the evolution of static instability and its relationship to the severe weather development are investigated. Several stability indices were calculated using the GALE supplemented sounding data to determine the potential for severe weather in this case. Results using the lifted index, total totals, and modified total totals indices are discussed in this section.

The lifted index (LI) was developed as a predictor of latent instability to aid in forecasting severe local storms (Galway 1956). The lifted index is the temperature at 500 mb minus the temperature of a parcel representing the average potential temperature, mixing ratio, and pressure of the lowest 100 mb of the sounding after it is lifted to 500 mb, dry adiabatically or moist adiabatically as appropriate. Lifted-index values $\leq 0$ are associated with severe thunderstorms and tornadoes over the eastern two-thirds of the United States (David and Smith 1971). A lifted index value of $-2$ was given as an upper bound for severe-storm formation in the Miller forecasting scheme (Miller 1967, 1972).

The static form (Sadowski and Rieck 1977; Lamb and Peppler 1985) utilizes the average potential temperature of the surface layer from current soundings, and does not take into account diurnal heating and moistening of the surface boundary layer. The static lifted index values for 1200 UTC (Fig. 20a) suggest that the potential for severe storms to form is limited to southern South Carolina and eastern Georgia. The

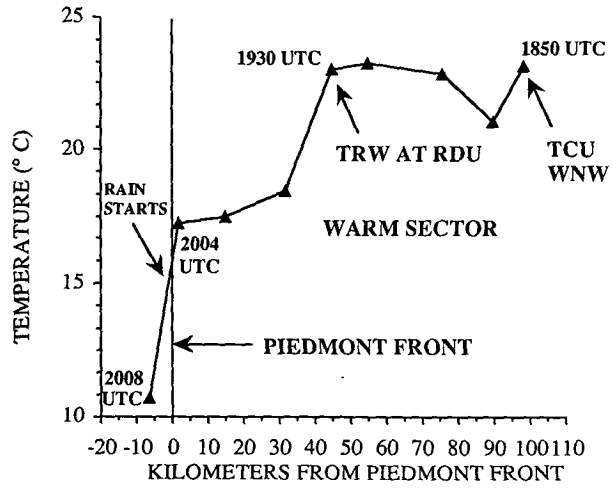


FIG. 19. Transect of squall line by instrumented automobile showing temperature trace taken on 13 March 1986.

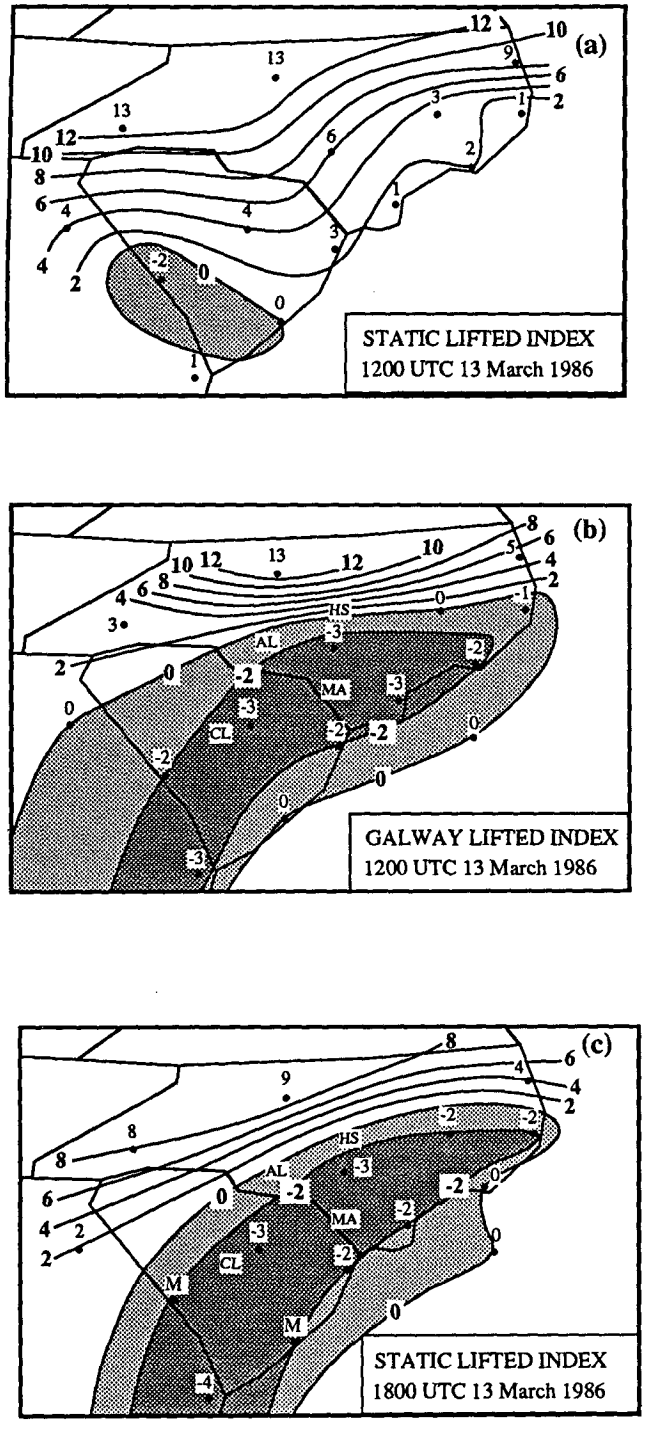


FIG. 20. (a) Static lifted index for 1200 UTC 13 March 1986. Shaded area indicates negative values. (b) Galway lifted index for 1200 UTC 13 March 1986. Lightly shaded area indicates values between 0 and −2, dark-shaded area indicates values < −2. (c) Static lifted index for 1800 UTC 13 March 1986. Lightly shaded area indicates values between 0 and −2, dark-shaded area indicates values < −2. AL, HS, CL, and MA indicate the locations of the reported severe thunderstorms.

sounding for Greensboro, North Carolina (GSO), at 1200 UTC 13 March (Fig. 21a) shows a strong, but shallow frontal inversion associated with the Piedmont front that results in a large positive value for the static lifted index (LI = 13). At 1200 UTC, the FAY sounding (Fig. 21b) shows a moist layer (~100 mb deep) within the frontal zone near the ground, with dry air at midlevels.

Between 1200 and 1800 UTC, eastern North Carolina experienced strong surface diabatic heating, and moisture advection at midlevels. An alternate method of calculating the lifted index uses the observed mean mixing ratio of an air parcel in the lowest 100 mb of the atmosphere, and the potential temperature corresponding to the dry adiabat passing through a predicted afternoon maximum temperature (Galway 1956). This method is often applied to the morning soundings (1200 UTC) by operational meteorologists in predicting afternoon thunderstorms. The Galway lifted index for 1200 UTC 13 March 1986 (using MOS-predicted afternoon maximum temperatures) indicates conditions conducive for severe storm formation over a much broader area, including eastern Georgia, most of South Carolina, and southeastern North Carolina (Fig. 20b). This formulation more accurately reflects the observed thunderstorm outbreak in this case. Severe thunderstorms at Holly Springs, Marietta, and Columbia all formed in the region of LI < −2. The distribution of Galway lifted index values in Fig. 20b shows a close correlation to the static lifted index calculated for 1800 UTC (Fig. 20c) near the time of maximum surface temperatures. The FAY sounding for 1800 UTC (Fig. 21c), when the thunderstorms were developing, shows a surface temperature of 27°C and static instability in the lower 150 mb, indicative of the effects of diabatic heating. The *K* index (George 1960) calculated for the FAY sounding at 1800 UTC was 36, indicating an 80%–90% probability of airmass thunderstorm activity. Use of forecast maximum temperatures was critical to the calculation of a lifted index representative of afternoon severe-weather potential, due to strong solar insolation and warm advection south of the Piedmont front.

The formation of the severe storm at Albemarle in a region with a static lifted index ~ +1 illustrates a limitation inherent in the formulation of the lifted index. Cold air at low levels north of the Piedmont front result in stable lifted index values, yet warm air overrunning the front can be lifted to its level of free convection. The total totals index (TT) usually avoids this problem by combining temperature and dewpoint temperature at the 850-mb level (which is above the Piedmont front) and 500-mb level (Miller 1967):

$$TT = T_{850} + T_{d850} - 2T_{500}.$$

Here $T$ and $T_d$ are the temperature and dewpoint temperature at the indicated pressure levels. As summa-

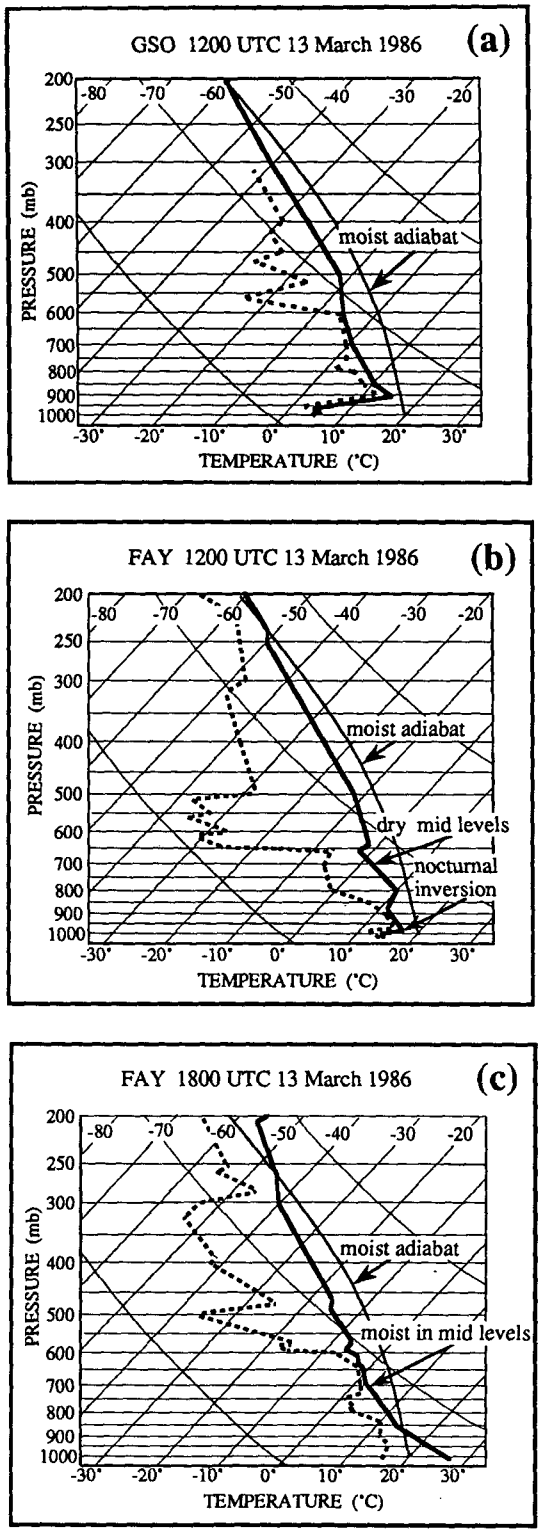


FIG. 21. Skew $T$-log$p$ plots: temperature curve (solid line) and dewpoint curve (dashed line). Isotherms slope from lower left to upper right. Moist adiabats slope from lower right to upper left. (a) Greensboro, North Carolina, at 1200 UTC 13 March 1986. (b) Fayetteville, North Carolina, at 1200 UTC 13 March 1986. (c) Fayetteville, North Carolina, at 1800 UTC 13 March 1986.

rized by Peppler (1988), Miller (1975) found TT = 44 to be the lower threshold value for the occurrence of isolated light thunderstorms, while values >60 indicated numerous moderate thunderstorms and scattered severe thunderstorms and tornadoes. The total totals index is used by Miller in his composite severe-storm forecast parameter charts. In this scheme, the likelihood of severe-storm development is considered "weak" if TT $\leq$ 50, "moderate" if 50 $\leq$ TT $\leq$ 55, and "strong" if TT $\geq$ 55.

The TT pattern for early afternoon (1800 UTC) on 13 March is shown in Fig. 22a. The locations of the severe weather events in the eastern Carolinas are all in the vicinity of the maximum TT $\sim$ +48. The above criteria would indicate only a "weak" chance of severe weather.

A modified total totals index (TTMOD) was introduced by Charba (1977), and found to be the single best predictor of severe local storms in the 2–6 h MOS forecasts (Charba 1979). In the above TT formula the 850-mb temperature and dewpoint temperature are replaced by simple averages of these variables at the surface and 850 mb. TTMOD values will thus be much more sensitive than TT to diurnal temperature variation. TTMOD values are typically larger than the corresponding TT values. However, a near-surface inversion can reverse the relative values of the two indices. On the relationship of TTMOD to thunderstorm probability Peppler (1988) notes that values indicative of thunderstorms and severe weather should be somewhat higher than comparable values of the total totals index.

Figure 22b shows the TTMOD pattern at 1800 UTC. The maximum in eastern North Carolina and South Carolina now has values somewhat in excess of 58. The minimum in western Virginia and North Carolina is more prominent than in the TT pattern in part because the shallow frontal inversion over this region has produced values of TTMOD less than TT (e.g., compare index values at stations PTB, GSO, AVL).

Since TTMOD is a measure of positive buoyant energy, large hail is the most closely correlated form of severe weather. Therefore, it is consistent that the reports of large hail at Marietta, North Carolina, and Columbia, South Carolina, occurred within the region of maximum TTMOD (Fig. 22b). The values here ($\sim$58) suggest a slight to moderate chance of severe weather occurrence based on this parameter alone. The implied probability of storm formation dramatically increased with solar heating. At station FAY, for example, TTMOD increases from 45 at 1200 UTC to 58 at 1800 UTC.

Conversely, station GSO located in the cloudy air west of the surface front only increases from 41 to 43 over the same 6 h. Thus, the two other severe weather occurrences, at Albemarle ($\sim$1900 UTC) and Holly Springs ($\sim$2000 UTC), have a less clear relationship with TTMOD, which would predict only a slight

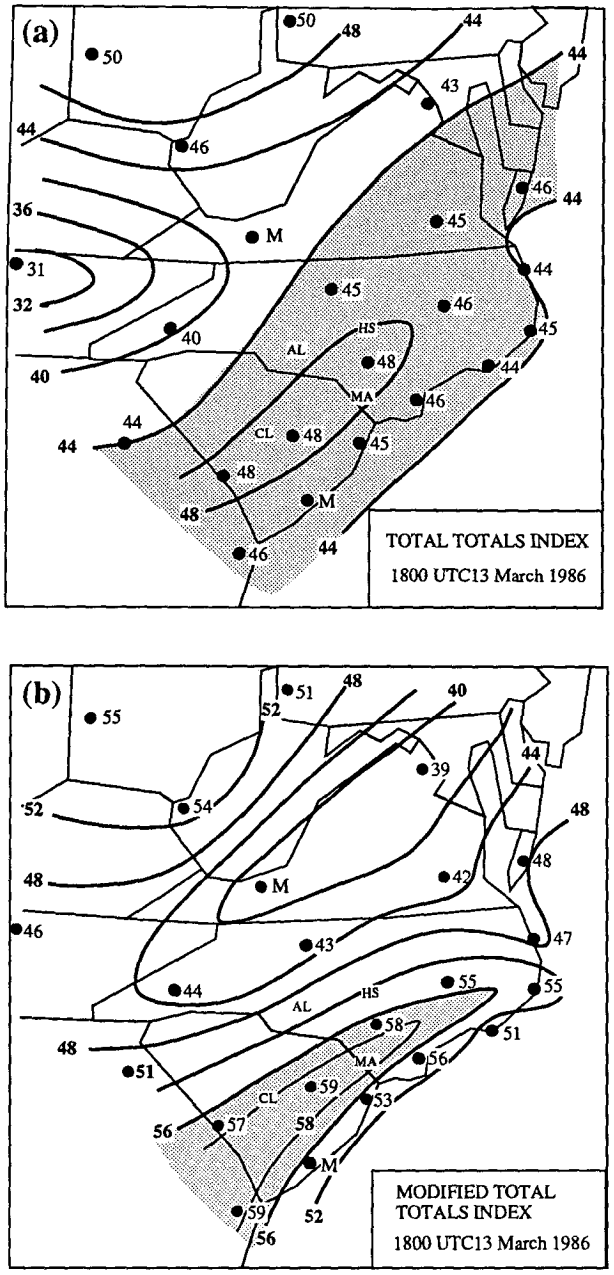


FIG. 22. (a) Total totals index for 1800 UTC 13 March 1986. Shaded area indicates the region for which the threshold value for the occurrence of isolated light thunderstorms has been reached. (b) Modified total totals index for 1800 UTC 13 March. Shaded area indicates threshold value for a moderate probability of severe thunderstorm occurrence. AL, HS, CL, and MA indicate the locations of the reported severe thunderstorms.

chance of severe thunderstorms. Strong straight-line winds observed with these two events suggest the presence of a destabilizing mechanism in addition to solar heating. The 1800 UTC GSO sounding (not shown) shows relative humidity <30% above 625 mb, with southwest winds >25 m $s^{-1}$. This high momentum stream of dry air at midlevels likely contributed to the strong straight-line winds reported with the Albemarle and Holly Springs storms (e.g., Ludlam 1963; and Fujita 1981). In the next section the role of kinematic forcing associated with the Piedmont front will be discussed.

## 7. Surface moisture-flux divergence and vertical motion

Moisture-flux convergence ($S_v < 0$) has long been recognized as essential to convection (e.g., Kuo 1965), and Charba (1979) found this quantity second only to TTMOD as a MOS predictor of local severe weather. Case studies (e.g., Waldstreicher 1989) have shown that storms often form in areas where moisture-flux convergence is increasing rapidly with time, and where the gradient in moisture-flux convergence is tightening. The two-dimensional moisture-flux divergence at the surface is given by

$$S_v = \nabla \cdot (\rho_v \mathbf{V}) = \frac{\partial(\rho_v u)}{\partial x} + \frac{\partial(\rho_v v)}{\partial y}.$$

Here $\rho_v$ is the absolute humidity or vapor density, and can be calculated from the equation of state for water vapor given the temperature and dewpoint temperature. These latter two variables and the wind components are objectively interpolated from the PAM II data to the Barnes analysis grid (see the Appendix for details).

Hourly patterns of $S_v$ from 1800 to 2200 UTC 13 March are shown in Fig. 23. The close association of maximum convergence ($S_v < -0.2$ g $m^{-3}$ $h^{-1}$) with the front and the weak low pressure systems moving along it is evident. Considering $S_v$ alone, its relationship to the four severe weather events is striking. The high wind events at Albemarle and Holly Springs formed in areas of enhanced kinematic ($S_v$) forcing, in the presence of high-momentum dry air at midlevels (Figs. 23b,c), while the large hail events at Marietta and Columbia formed in areas favored by both thermodynamic (Fig. 22b) and kinematic (Fig. 23c) forcing. The linear pattern of enhanced moisture-flux convergence along the Piedmont front at the later times (Figs. 23d,e) is consistent with the emergence of the squall line (see Fig. 16e).

To investigate the influence of vertical motion patterns on the development of the severe weather and cyclogenesis along the Piedmont front in this case, two methods of diagnosing the vertical velocity field (quasi-geostrophic and kinematic) (Holton 1979) are contrasted below.

### *a. Quasi-geostrophic method*

The quasi-geostrophic omega equation in isobaric coordinates provides a diagnostic means of determining the vertical velocity field. As discussed in Trenberth (1978), one can ignore the difference between the advection of relative and absolute vorticity and approx-

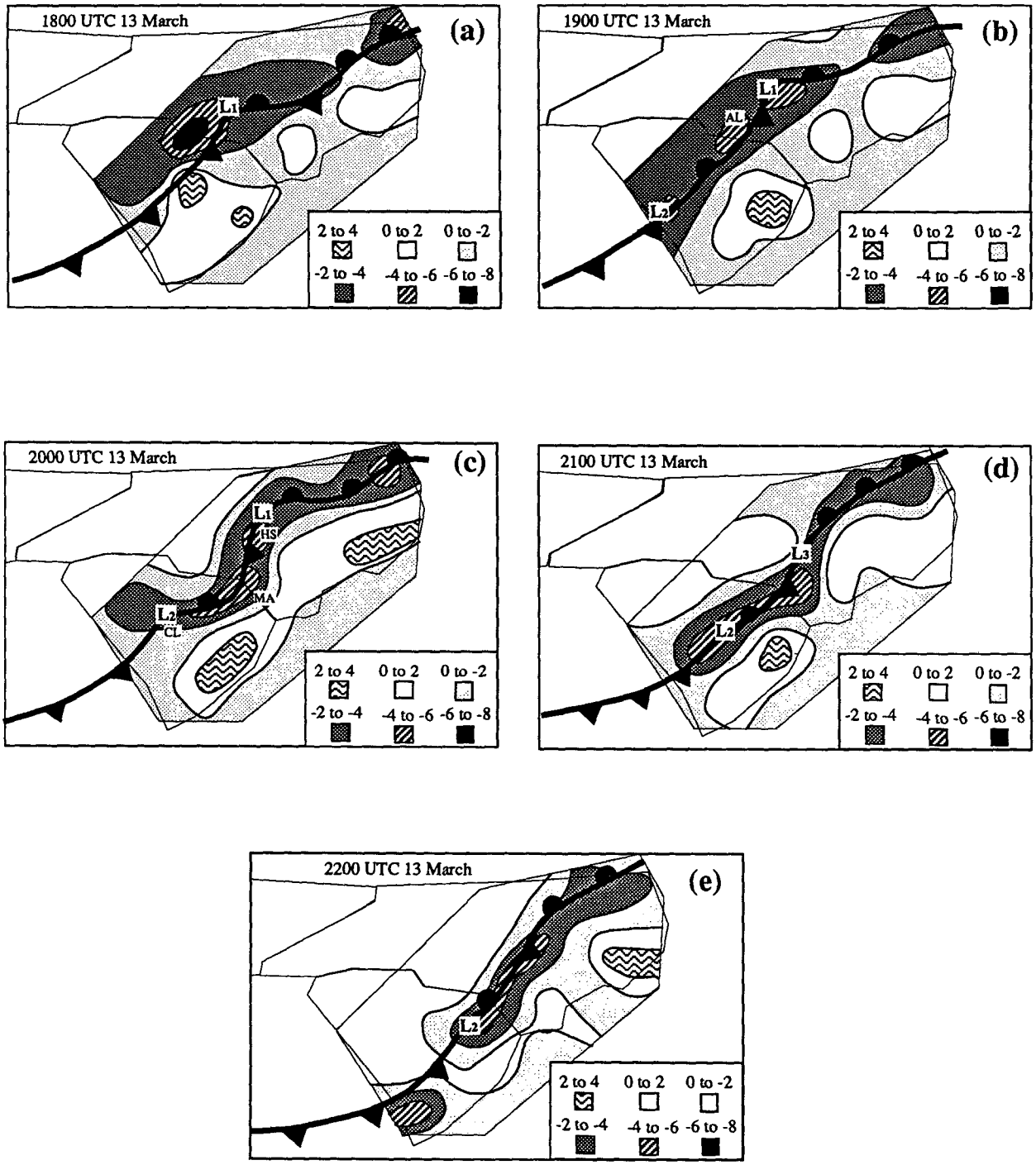


FIG. 23. Moisture-flux divergence ($10^{-1}$ g m$^{-3}$ h$^{-1}$) for (a) 1800 UTC, (b) 1900 UTC, (c) 2000 UTC, (d) 2100 UTC, and (e) 2200. AL, HS, CL, and MA indicate the locations of the reported severe thunderstorms.

imate the omega equation with minimal loss of accuracy as:

$$\left(\sigma\nabla^2 + f_0^2\frac{\partial^2}{\partial p^2}\right)\omega = 2f_0\frac{\partial \mathbf{V}_g}{\partial p}\cdot\left(\nabla\frac{1}{f_0}\nabla^2\phi\right) + (\text{terms involving the deformation of the wind field}).$$

In this equation $\sigma$ is static stability, $f_0$ is constant Coriolis parameter at 35°N, $\omega$ is vertical velocity in isobaric coordinates, $\mathbf{V}_g$ is the geostrophic wind, $\phi$ is geo-

potential, and $p$ is the pressure. The gradient and Laplacian operators are two-dimensional in $x$ and $y$. When applied in the middle troposphere, Trenberth showed that the right-hand side of the above equation is dominated by the contribution from the advection of vorticity by the thermal wind. Omega was analyzed at 700 mb because of the shallow nature of the Piedmont front (e.g., Fig. 21a), and to compare the forcing pattern with the vertical velocity patterns calculated using the kinematic method. The result (Fig. 24a) shows a region of enhanced positive vorticity advection (PVA, shaded) over western North Carolina extending south into central South Carolina. The western edge of the PVA coincides with the position of the CFA in Fig. 17.

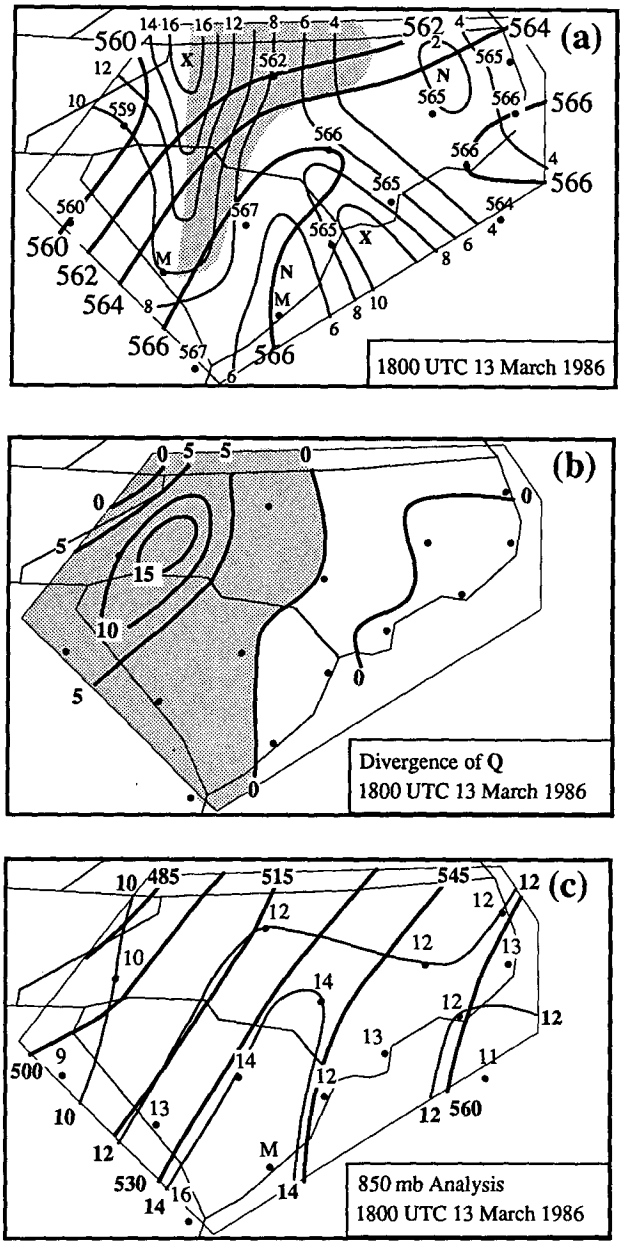


FIG. 24. 1800 UTC 13 March 1986: (a) 1000–500 mb thickness (bold contours every 60 m) and 700-mb absolute vorticity (thin contours every $2 \times 10^{-6}$ s$^{-1}$). Shading indicates region of positive vorticity advection. (b) Divergence of Q vector ($-2 \times \nabla \cdot \mathbf{Q}$) ($\times 10^{-18}$ m kg$^{-1}$ s$^{-1}$) for the 700-mb level at 1800 UTC 13 March 1986. (c) Analysis of 850-mb heights (bold contours every 15 dam) and temperature (thin contours every 2°C). Station reports include temperature (°C).

Another method of viewing geostrophic forcing of vertical motion is divergence of the Q vector (Hoskins et al. 1978). The authors show that the omega equation can be written:

$$\left(\sigma\nabla^2 + f_0^2 \frac{\partial^2}{\partial p^2}\right)\omega = -2\nabla \cdot \mathbf{Q}.$$

Where the $x$, $y$ components of Q are given by:

$$\mathbf{Q} = \left[\frac{\partial \mathbf{V}_g}{\partial x} \cdot \nabla\left(\frac{\partial \Phi}{\partial p}\right), \frac{\partial \mathbf{V}_g}{\partial y} \cdot \nabla\left(\frac{\partial \Phi}{\partial p}\right)\right].$$

The symbols are as defined above. The Q vector provides an approximate picture of the ageostrophic horizontal wind in the lower branch of the circulation that develops in order to maintain thermal-wind balance in an evolving synoptic disturbance (Hoskins and Pedder 1980). Convergence of the Q vector (positive forcing) implies ascending motion ($\omega < 0$); divergence of Q (negative forcing) implies subsidence ($\omega > 0$).

Figure 24b shows the 700-mb pattern of divergence of Q for 1800 UTC 13 March. The greatest forcing for upward motion (shaded area) is located across the western Carolinas just ahead of the approaching CFA (see Fig. 17). Little or no forcing is evident over central and eastern North Carolina and South Carolina at this time.

Figure 24c shows the height and temperature analysis for 850 mb at 1800 UTC. At this time the Carolinas are dominated by southerly flow at 850 mb. Geostrophic cold advection associated with the CFA can be seen over the westernmost portions of North and South Carolina, with a tongue of warm advection further east. No evidence of the Piedmont front is seen in the thermal field at this level over the Carolinas due to the shallow nature of this front (e.g., Fig. 21a). Confluence acting on the temperature field over western North Carolina is consistent with the maximum in upward forcing seen in Figs. 24a and b.

### *b. Kinematic method*

Vertical velocity at the top of a column of any depth in the atmosphere can be calculated using the continuity equation in isobaric coordinates by integrating the divergence of the horizontal wind field with height after specifying a lower boundary condition (Holton 1979). The density of sounding data during GALE (see Fig. 3a) gives an opportunity to diagnose subsynoptic-scale aspects of the vertical velocity field for this case. The lower boundary condition for the calculations presented in this section was taken as the vertical ve-

locity resulting from flow normal to the surface slope in the inner GALE area. The primary drawback of the kinematic method is its sensitivity to subgrid scales of real variability and to errors in the observed winds. Systematic accumulation of error in the divergence with height results in an over- or underestimate of the vertical motion in the upper troposphere. The effect of this systematic error was reduced by considering only results in the lower troposphere ($\geqslant$700 mb), and by utilizing an adjustment scheme (O'Brien 1970) which constrains $\omega$ to zero at the 100-mb level, while linearly adjusting the divergence.

The lowest pressure surface with data reported by the higher-elevation rawinsonde stations (AHN, AVL, and GSO in Fig. 3a) is 940 mb in this case. In the practical use of the kinematic method, the pressure thickness of the lowest layer in the vertical integration is defined by the surface and the 940-mb isobaric level. This assures that the objective analysis will provide meaningful mean layer divergence and vertical motion computations over the western portion of the inner GALE region.

Figure 25a depicts the 850-mb kinematic omega for 1800 UTC. Observed horizontal winds show strong directional confluence over western South and North Carolina at this level, which contributes to the axis of greatest upward motion along the Piedmont frontal position. The maximum upward motion ($\omega < -8$ $\mu$b s$^{-1}$) occurs just west of the surface mesolow, and is consistent with the maximum moisture-flux convergence seen over this region in Fig. 23a. It is noteworthy that the severe thunderstorm cell at Albemarle formed in this same vicinity during the following hour.

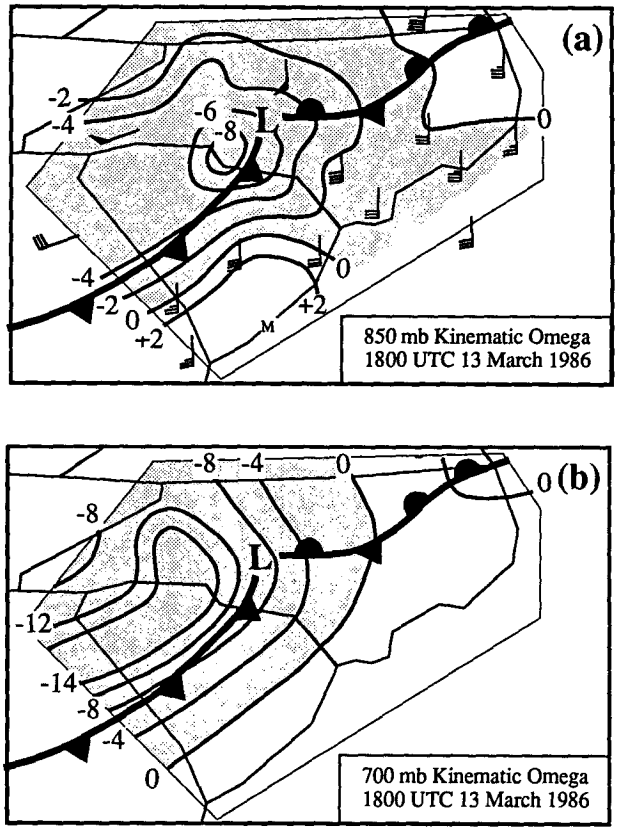


FIG. 25. Kinematic omega and surface fronts for 1800 UTC 13 March 1986. Shaded areas indicate upward vertical motion. Solid contours are vertical velocities ($\mu$b s$^{-1}$). (a) Kinematic omega and winds at 850-mb level (1/2 barb = 2.5 m s$^{-1}$, barb = 5 m s$^{-1}$, and pennant = 25 m s$^{-1}$). (b) Kinematic omega at 700-mb level.

Figure 25b depicts the 700-mb kinematic omega for 1800 UTC. The magnitude of the upward vertical velocities has increased at this level, with maximum values occurring northwest of the Piedmont front over western North and South Carolina. This pattern is in general agreement with that implied by Q-vector analysis at this level (Fig. 24b), although the maximum upward vertical velocities are slightly to the southeast of the maximum geostrophic forcing.

In comparing the broad pattern of calculated vertical motion (Figs. 25a) and observed radar reflectivity (Fig. 16b), the subsynoptic pattern of upward motion is in good agreement with the squall line over Georgia and South Carolina and position of the CFA (see Fig. 17). A lack of a one-to-one correlation on the meso-$\beta$ scale over eastern South and North Carolina reflects the convective character of the precipitation and limitations in the resolution of the sounding data employed. Given a general eastward propagation of the vertical velocity pattern, the four severe thunderstorms that formed during the following 2 h all occurred in a region of moderate upward motion ($\omega < -4$ $\mu$b s$^{-1}$).

## 8. Discussion and conclusions

The research presented in this paper documents the complex interaction between observed frontogenesis, cyclogenesis, severe weather development, and squall-line formation on 13 March 1986. An objective analysis scheme was utilized in analysis of data from varied observation networks deployed during the field phase of the Genesis of Atlantic Lows Experiment (GALE).

Surface high pressure over New England on 12 March resulted in cold-air damming along the eastern slopes of the Appalachians, providing a synoptic pattern conducive to frontogenesis over the Carolinas. Mesoscale analysis reveals that a sharp surface front rapidly developed along an axis of dilatation over the eastern margin of the Piedmont on 13 March, while a coastal front dissipated over the cool nearshore waters. As surface frontogenesis progressed, a continuous *Piedmont front* emerged. The observed spatial and temporal scales of the frontogenesis are significantly smaller than predicted by semigeostrophic models (as in Hoskins and Bretherton 1972). Pinkerton (1978), in a two-dimensional numerical study that incorporated PBL parameterization, showed that the scale of the cross-frontal circulation contracted significantly for simu-

lations in which the sensible heat flux was larger on the warm side of the front. In the present case a complete overcast on the cold side of the front and only partial cloud cover on the warm side of the front during the morning of 13 March resulted in differential insolation across the front, which may help explain the scale of the observed frontogenesis.

Near the time of maximum frontogenesis a line of convection and a clear zone appeared in the satellite imagery (Fig. 18). Previous research (Koch 1984) has documented the possible role of mesoscale transverse circulations about cold fronts in the formation of clear zones and the initiation of a squall line in the downward and upward branches of the circulation, respectively. Dorian and Koch (1988) have explored the potential of using clear zones associated with cold fronts as a short term predictor of squall-line formation. However, in the present case, the convective line and clear zone both originate to the east of the surface front.

Stability analysis revealed that on the synoptic scale only a slight to moderate potential for severe weather existed over the Carolinas on the afternoon of 13 March. Subsequently, the locations of four severe thunderstorms that developed were closely linked to mesoscale patterns of forcing. The first storm developed at Albemarle, North Carolina, and produced high surface winds. It was triggered just west of and above the Piedmont front, in an area of enhanced moisture flux convergence. Nearby (GSO) sounding data indicate the presence of a high momentum stream of dry air at midtropospheric levels, that likely contributed to the intensity of downdrafts through evaporational cooling. In addition, a maxima in upward motion was diagnosed in the lower troposphere over this region in association with a mesoscale low pressure center (mesolow) that formed along the front.

Mesoscale cyclogenesis along shallow baroclinic zones has been documented previously (e.g., see Businger and Reed 1989). Moore and Peltier (1989), in a study using a primitive-equation numerical model, show that small amplitude perturbations on a shallow baroclinic zone are highly unstable, with the fastest growing disturbances exhibiting horizontal length scales on order of 500 km. Furthermore, they show that these disturbances display many features in common with the Norwegian cyclone model (Bjerknes and Solberg 1922), including the tendency to exist in cyclone families or wave trains. The absence of friction, however, is a limitation of their model. Fujita (1955) documented mesolows that develop in response to subsidence warming in the dry air to the rear of the precipitation zone associated with convective lines. Fujita's mesolows are, however, almost always accompanied by a strong mesohigh development that is not observed in this case (Fig. 14a). Moreover, there is evidence in the surface wind observations of the existence of the mesolow prior to the development of the convection in this case.

Severe thunderstorms that struck Holly Springs, North Carolina, and Columbia, South Carolina, also formed in the near vicinity of mesolows (Fig. 23c). These storms, as well as the storm that passed Marietta, North Carolina, developed just on the warm side of the Piedmont front in areas also characterized by enhanced moisture-flux convergence. The storms at Columbia and Marietta produced large hail, indicative of strong updrafts. Consistent with the need for large buoyancy, these storms formed along an axis of minimum stability that developed in the afternoon over the Carolina coastal plain (Fig. 22). The storm at Holly Springs resulted in strong surface winds. Its location further north placed it nearer to the axis of strongest midtropospheric winds; a source of high momentum dry air (Fig. 24).

A second line of convection formed to the west of the Piedmont front, in unstable air overrunning the front. This line formed just ahead of a pool of cooler, drier air advancing from the southwest at midtropospheric levels. The leading edge of this drier air has been analyzed as a cold front aloft (CFA), and its history can be traced to a cold front and short wave that crossed the Pacific coast two days previously (Hobbs et al. 1990). Although the strength of the CFA gradually weakened as it propagated eastward, it was still discernable in the temperature and wind fields over Georgia and the Carolinas at 1800 UTC 13 March (Fig. 17). Diagnostics of the vertical motion field indicate that conditions conducive to upward vertical motion were present ahead of the CFA and over the Piedmont front. As the second convective line and the Piedmont front merged with the initial line of convection to the east, a squall line emerged over the coastal plain. The squall line was characterized by a well-defined band of enhanced precipitation. As evening approached, and the squall line advanced toward the cool nearshore waters along the coast, it dissipated.

A three-dimensional schematic model was constructed to portray key physical elements in the state of the atmosphere at the onset of severe weather and squall-line formation (Fig. 26). The point of the model is to draw attention to those signatures of the environment in this case study that may provide keys to improved forecasting of similar events in the future. The key elements of the schematic model include:

(a) a warm, moist low-level flow of air off the Atlantic Ocean and cold-air damming further west resulting in strong low-level frontogenesis.

(b) Differential solar insolation across the Piedmont front with enhanced insolation on the warm side.

(c) Pronounced moisture-flux convergence at the surface in the vicinity of the Piedmont front.

(d) A southwesterly flow of dry, cool air aloft associated with a CFA, with subsynoptic upward forcing of vertical motion ahead of the CFA.

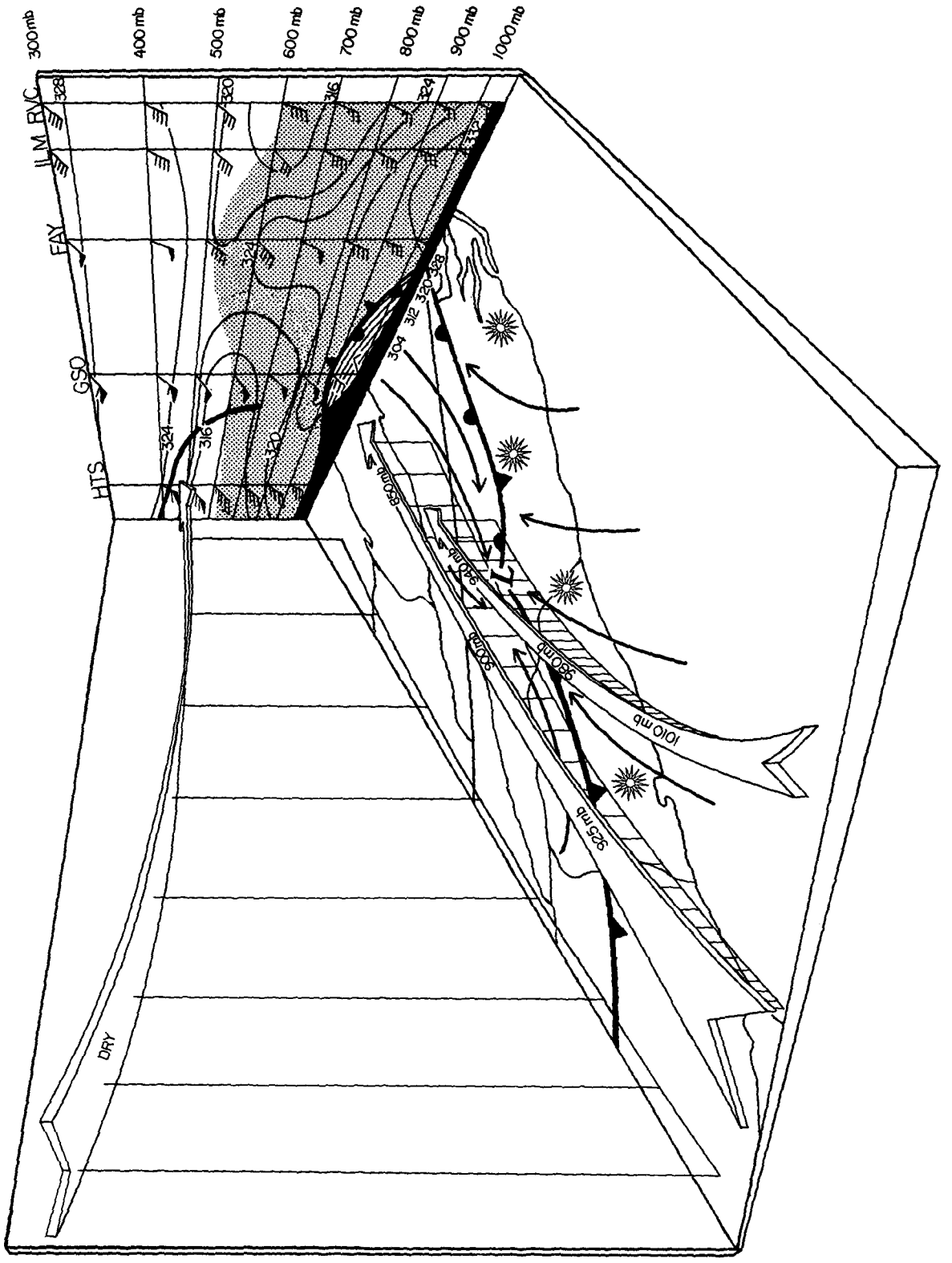


FIG. 26. Schematic at time of the severe-weather outbreak (1800 UTC 13 March 1986). The Piedmont front is depicted with the conventional frontal symbols, solid arrows indicate surface streamlines, open arrows indicate calculated airflow trajectories aloft. Sun symbols indicate area of strongest diabatic heating due to solar insolation and the "L" indicates the location of a mesolow. The back wall shows the 1800 UTC cross section from RVC to FAY (refer to Fig. 3a for location); contours are equivalent potential temperature (K), rawinsonde winds are shown with the usual convention, shading indicates the area with decreasing equivalent potential temperature with height, and the heavy solid line indicates the approximate position of the CFA.

The first two elements above, in a synoptic pattern conducive to cold-air damming, combined to produce a sharp surface front over the eastern margin of the Piedmont of the Carolinas. (Note the shallow extent of the Piedmont front in Fig. 26.) Four severe thunderstorms were initiated in weak to moderately unstable air in areas of enhanced moisture-flux convergence in the vicinity of the front. Subsequently, upward forcing of vertical motion ahead of the CFA aided in the formation of a squall line over North Carolina characterized by a well-defined linear band of enhanced precipitation along the Piedmont front.

*Acknowledgments.* The authors wish to thank Mr. John Locatelli for drawing attention to the importance of the cold front aloft in this case, and Dr. Richard Reed for constructive conversations concerning the research. We also wish to express appreciation to William F. Roberts for providing radar mosaics and Mary McVicker for assistance in drafting of the figures. The authors are indebted to Fred Sanders and to two anonymous reviewers for their constructive reviews. This material was based upon work supported by the National Science Foundation under Grants ATM-8318857 and ATM-8421396-01.

## APPENDIX

### Objective Analysis Scheme and Numerical Computations

If $Q$ represents any meteorological variable, calculations of gridpoint values are obtained by (Barnes 1964 and 1973):

$$\bar{Q} = \sum_{i=1}^{N} w_i Q_i / \sum_{i=1}^{N} w_i .$$

The interpolated gridpoint value is the weighted mean ($\bar{Q}$) of observations surrounding the point, $N$ is the total number of stations influencing a given grid point, $w_i$ is the observation weight, and $Q_i$ is the observed value. The observation weights $w_i$ are inverse-distance $d$ dependent and are defined by: $w_i = \exp(-d^2/4k_0)$. Here $k_0$ is the "weight parameter" which controls the rate at which the weight value decreases outward from the point of interpolation. Hence, $k_0$ determines the degree of smoothing of the data field: if $k_0$ is small, there is little smoothing; if $k_0$ is large, there is greater smoothing.

The appropriate choice of $k_0$ can be determined by selecting the amplitude suppression (response function) of the minimally resolved wavelength, the latter being twice the average station spacing. The station spacing of the GALE PAM II network is ~68 km, while that of the inner area sounding network (CLASS plus local NWS stations) is ~180 km. If both surface and upper-air minimally resolved waves are suppressed to about 16% of their initial amplitude, the two-pass Barnes theory suggests weight parameters of about 2900 km$^2$ and 20 000 km$^2$, respectively. To obtain these values a convergence parameter $\gamma = 0.3$ is used in the second pass. In the second pass the weight is reduced to $\gamma k_0$ and the above weighted mean applied to the difference in the observation and the first-pass interpolated values at the stations. The amplitude response adopted in this study is consistent with those chosen in other recent applications of the Barnes scheme (Barnes 1985, 15%; Moore and Blakely 1988, 21%).

All finite-difference calculations were standard second-order centered differences. Objectively interpolated values of temperature and wind components were obtained over a 17 × 21 grid centered over the inner GALE observation network (Fig. 3b). The grid spacing at the mean latitude of the grid (35°N) is about half the PAM II station spacing (~34 km). This same grid is retained in upper-air calculations.

To minimize analysis and computation errors around the edges of the inner GALE area (generally defined by the PAM II network), observations by surrounding station networks were included in the objective analysis. At the surface, these supplemental data included the standard hourly surface network plus available ships and buoys. Aloft, the analysis network included the regional GALE area sounding stations plus ship soundings (RV *Cape Hatteras*) and available offshore Omega dropsondes.

## REFERENCES

Ballentine, R. J., 1980: A numerical investigation of New England coastal frontogenesis. *Mon. Wea. Rev.*, **108**, 1479–1497.

Barnes, S. L., 1964: A technique for maximizing details in numerical weather map analysis. *J. Appl. Meteor.*, **3**, 396–409.

——, 1973: Mesoscale objective analysis using weighted time-series observations. NOAA Tech. Memo. ERL NSSL-62, Norman, OK, 60 pp.

——, 1985: Omega diagnostics as a supplement to LFM/MOS guidance in weakly forced convective situations. *Mon. Wea. Rev.*, **113**, 2122–2141.

Bell, G. D., and L. F. Bosart, 1988: Appalachian cold-air damming. *Mon. Wea. Rev.*, **116**, 137–161.

Betts, A. K., 1973: Nonprecipitating cumulus convection and its parameterization. *Quart. J. Roy. Meteor. Soc.*, **99**, 178–196.

Bjerknes, J., and H. Solberg, 1922: Life cycle of cyclones and the polar front theory of atmospheric circulation. *Geofys. Publ.*, **3**, 1–18.

Bosart, L. F., C. J. Vaudo and J. H. Helsdon, 1972: Coastal frontogenesis. *J. Appl. Meteor.*, **11**, 1236–1258.

——, 1973: Detailed analyses of precipitation patterns associated with mesoscale features accompanying United States east coast cyclogenesis. *Mon. Wea. Rev.*, **101**, 1–12.

——, V. Pagnotti and B. Lettau, 1973: Climatological aspects of eastern United States back door frontal passages. *Mon. Wea. Rev.*, **101**, 627–635.

——, 1975: New England coastal frontogenesis. *Quart. J. Roy. Meteor. Soc.*, **101**, 957–978.

Businger, S., and R. J. Reed, 1989: Polar Lows. *Polar and Arctic Lows*, P. F. Twitchell, E. A. Rasmussen and K. L. Davidson, Eds., A. Deepack Publishing, 3–45.

Carr, J. A., 1951: The East Coast backdoor cold front of 16–20 May 1951. *Mon. Wea. Rev.*, **79**, 100–105.

Charba, J. P., 1977: Operational scheme for short range forecasts of severe local storms two to six hours in advance. NOAA Tech. Memo. NWS TDL-5, 36 pp.

——, 1979: Two to six hour severe local storm probabilities: an operational forecasting system. *Mon. Wea. Rev.*, **102,** 268–282.

David, C. L., and J. S. Smith, 1971: An evaluation of seven stability indices as predictors of severe thunderstorms and tornadoes. Preprints, *Seventh Conf. Severe Local Storms,* Kansas City, Amer. Meteor. Soc., 105–109.

Dirks, R. A., J. P. Kuettner and J. A. Moore, 1988: Genesis of Atlantic Lows Experiment (GALE): an overview. *Bull. Amer. Meteor. Soc.*, **69,** 148–160.

Dorian, P. B., and S. E. Koch, 1988: Mesoscale frontogenesis as a predictor of squall line initiation. Preprints, *15th Conf. on Severe Local Storms,* Norman, OK, Amer. Meteor. Soc., 364–367.

Doswell, C. A., 1980: Synoptic environments associated with high plains severe thunderstorms. *Bull. Amer. Meteor. Soc.*, **61,** 1388–1400.

——, 1987: The distinction between large-scale and mesoscale contribution to severe convection: A case study example. *Wea. Forecasting,* **2,** 3–16.

Ertel, H., 1942: Ein neuer hydrodynamischer wirbelsatz. *Met. Z.*, **59,** 271–281.

Fawbush, E. J., R. C. Miller and L. G. Starrett, 1951: An empirical method of forecasting tornado development. *Bull. Amer. Meteor. Soc.*, **32,** 1–9.

Forbes, G. S., R. A. Anthes and D. W. Thompson, 1987: Synoptic and mesoscale aspects of an Appalachian ice storm associated with cold-air damming. *Mon. Wea. Rev.*, **115,** 564–591.

Fujita, T. T., 1955: Results of detailed synoptic studies of squall lines. *Tellus,* **7,** 405–436.

——, 1981: Tornadoes and downbursts in the context of generalized planetary scales. *J. Atmos. Sci.*, **38,** 1511–1534.

Galway, J. G., 1956: The lifted index as a predictor of latent instability. *Bull. Amer. Meteor. Soc.*, **37,** 528–529.

George, J. J., 1960: *Weather and Forecasting for Aeronautics.* Academic Press, 407–415.

Hobbs, P. V., J. D. Locatelli and J. E. Martin, 1990: Cold fronts aloft and the forecasting of precipitation and severe weather east of the Rocky Mountains. *Wea. Forecasting,* **5,** 613–626.

Holton, J. R., 1979: *An Introduction to Dynamic Meteorology.* International Geophysics Series, Vol. 23, Academic Press, 391 pp.

Hoskins, B. J., and F. P. Bretherton, 1972: Atmospheric frontogenesis models: Mathematical formulation and solution. *J. Atmos. Sci.*, **29,** 11–37.

——, I. Draghici and H. C. Davies, 1978: A new look at the omega-equation, *Quart. J. Roy. Meteor. Soc.*, **104,** 31–38.

——, and M. A. Pedder, 1980: The diagnosis of middle latitude synoptic development. *Quart. J. Roy. Meteor. Soc.*, **106,** 707–720.

Johns, R. H., 1984: A synoptic climatology of northwest-flow severe weather outbreaks. Part II: Meteorological parameters and synoptic patterns. *Mon. Wea. Rev.*, **112,** 449–464.

Keyser, D., and M. A. Shapiro, 1986: A review of the structure and dynamics of upper-level frontal zones. *Mon. Wea. Rev.*, **114,** 452–499.

Koch, S. E., 1984: The role of an apparent mesoscale frontogenetical circulation in squall line initiation. *Mon. Wea. Rev.*, **112,** 2090–2111.

Kuo, H. L., 1965: On the formation and intensification of tropical cyclones through latent heat release by cumulus convection. *J. Atmos. Sci.*, **22,** 40–63.

Lamb, P. J., and R. A. Peppler, 1985: Tropospheric static stability and central North America summer rainfall during 1979. *Proc. Ninth Annual Climate Diagnostics Workshop,* Washington, D.C., U.S. Department of Commerce, 274–283.

Ludlam, F. H., 1963: Severe local storms: A review. *Severe Local Storms, Meteor. Monogr.*, No. 27, Amer. Meteor. Soc., 247 pp.

Maddox, R. A., and C. A. Doswell, 1982: An examination of jetstream configurations, 500 mb vorticity advection, and low-level thermal advection patterns during extended periods of intense convection. *Mon. Wea. Rev.*, **110,** 184–197.

Marks, F. D., Jr., and P. M. Austin, 1979: Effects of the New England coastal front on the distribution of precipitation. *Mon. Wea. Rev.*, **107,** 53–67.

Martin, J. E., J. D. Locatelli and P. V. Hobbs, 1990: Organization and structure of clouds and precipitation on the mid-Atlantic coast of the United States. Part III: The evolution of a midtropospheric cold front. *Mon. Wea. Rev.*, **118,** 195–217.

Miller, J. E., 1948: On the concept of frontogenesis. *J. Meteor.*, **5,** 169–171.

Miller, R. C., 1967: Notes on analysis and severe storm forecasting procedures of the Military Weather Warning Center. Tech. Rep. 200, AWS, USAF, [Available from Headquarters AWS, Scott AFB, IL 62225.]

——, 1972: Notes on analysis and severe storm forecasting procedures of the Air Force Global Weather Central. Tech. Rep. 200 (Revised), AWS, USAF, [Available from Headquarters AWS, Scott AFB, IL 62225.]

——, 1975: Notes on analysis and severe storm forecasting procedures of the Air Force Global Weather Central. Tech. Rep. 200 (Revised), AWS, USAF, [Available from Headquarters AWS, Scott AFB, IL 62225.]

Moore, G. W. K., and W. R. Peltier, 1989: On the development of polar low wavetrains. *Polar Lows,* P. F. Twitchell, E. A. Rasmussen and K. L. Davidson, Eds. A. Deepack Publishing, 421 pp.

Moore, J. T., and P. D. Blakely, 1988: The role of frontogenetical forcing and conditional instability in the Midwest snowstorm of 30–31 January 1982. *Mon. Wea. Rev.*, **116,** 2155–2171.

Nielsen, J. W., 1989: The formation of New England coastal fronts. *Mon. Wea. Rev.*, **117,** 1380–1401.

——, and P. P. Nielley, 1990: The vertical structure of New England coastal fronts. *Mon. Wea. Rev.*, **118,** 1793–1807.

NOAA, 1981: Weather radar observations, *Federal Meteorological Handbook No. Seven,* USDC/NOAA, 256 pp.

——, 1986: Storm data. *NOAA Tech. Rep.*, **28,** 31–34.

O'Brien, J. J., 1970: Alternative solutions to the classical vertical velocity problem. *J. Appl. Meteor.*, **9,** 197–203.

Peppler, R. A., 1988: A review of static stability indices and related thermodynamic parameters. Illinois State Water Survey miscellaneous publication 104, Climate and Meteorology Section, Illinois State Water Survey, Champaign, IL, 87 pp.

Petterssen, S., 1956: *Weather Analysis and Forecasting.* Vol. I. McGraw Hill, 428 pp.

Pinkerton, J. E., 1978: Numerical experiments on boundary layer effects on frontal structure. Ph.D. thesis, Drexel University, 213 pp.

Purdom, J. F., 1979: The development and evolution of deep convection. Preprints, *11th Conf. on Severe Local Storms,* Kansas City, Amer. Meteor. Soc., 143–150.

Reed, R. J., 1955: A study of a characteristic type of upper-level frontogenesis. *J. Meteor.*, **12,** 226–237.

——, and F. Sanders, 1953: An investigation of the development of a midtropospheric frontal zone and its associated vorticity field. *J. Meteor.*, **10,** 338–349.

Richwein, B. A., 1980: The damming effect of the southern Appalachians. *Natl. Wea. Dig.*, **5,** 2–12.

Riordan, A. J., 1990: Examination of the mesoscale features of the GALE coastal front of 24–25 January 1986. *Mon. Wea. Rev.*, **118,** 258–282.

Sadowski, A. F., and R. E. Rieck, 1977: Stability indices. NOAA NWS TPB-207, 8 pp.

Saucier, W. J., 1955: *Principles of Meteorological Analysis.* Dover Publications, 438 pp.

Trenberth, K. E., 1978: On the interpretation of the diagnostic quasi-geostrophic omega equation. *Mon. Wea. Rev.*, **106,** 131–137.

Uccellini, L. W., and D. R. Johnson, 1979: The coupling of upper and lower tropospheric jet streaks and implications for the development of severe convection. *Mon. Wea. Rev.*, **107,** 682–703.

Waldstreicher, J. S., 1989: A guide to utilizing moisture flux convergence as a predictor of convection. *Natl. Wea. Dig.*, **14,** 20–35.